Pion transverse momentum dependent parton distributions in a light-front constituent approach, and the Boer-Mulders effect in the pion-induced Drell-Yan process

B. Pasquini[1,2] and P. Schweitzer[3]

[1]*Dipartimento di Fisica, Università degli Studi di Pavia, I-27100 Pavia, Italy*
[2]*Istituto Nazionale di Fisica Nucleare, Sezione di Pavia, I-27100 Pavia, Italy*
[3]*Department of Physics, University of Connecticut, Storrs, Connecticut 06269, USA*

(Received 16 June 2014; published 28 July 2014)

At leading twist the transverse momentum dependent parton distributions of the pion consist of two functions, the unpolarized $f_{1,\pi}(x,\boldsymbol{k}_\perp^2)$ and the Boer-Mulders function $h_{1,\pi}^\perp(x,\boldsymbol{k}_\perp^2)$. We study both functions within a light-front constituent model of the pion, comparing the results with different pion models and the corresponding nucleon distributions from a light-front constituent model. After evolution from the model scale to the relevant experimental scales, the results for the collinear pion valence parton distribution function $f_{1,\pi}(x)$ are in very good agreement with available parametrizations. Using the light-front constituent model results for the Boer-Mulders functions of the pion and nucleon, we calculate the coefficient ν in the angular distribution of Drell-Yan dileptons produced in pion-nucleus scattering, which is responsible for the violation of the Lam-Tung relation. We find a good agreement with the data, and carefully discuss the range of applicability of our approach.

DOI: 10.1103/PhysRevD.90.014050 PACS numbers: 12.39.Ki, 13.60.Hb, 13.85.Qk

I. INTRODUCTION

Transverse momentum dependent distribution functions (TMDs) [1–3] provide unique insights into the 3D hadronic structure [4–8], by taking into account the transverse motion of partons and spin-orbit correlations. The Drell-Yan process (DY) [9,10] is basically the only source for this type of information for hadrons other than the nucleon, that are available as secondary beams in high energy experiments, such as the pion which is the main focus of this work. DY experiments with pions were reported in Refs. [11–16], see [17] for a compilation of DY data till 1993 and [18–22] for reviews of later data and theoretical progress. TMDs describe hard processes like DY on the basis of factorization theorems [23–26]. The QCD evolution properties of some of the TMDs were studied in Refs. [3,27–33].

This work is devoted to the study of leading-twist TMDs of the pion. At leading twist the pion structure is described in terms of two TMDs, $f_{1,\pi}(x,\boldsymbol{k}_\perp^2)$ and $h_{1,\pi}^\perp(x,\boldsymbol{k}_\perp^2)$. The unpolarized TMD $f_{1,\pi}(x,\boldsymbol{k}_\perp^2)$ describes the distribution of unpolarized partons carrying the longitudinal momentum fraction x of the pion, and the transverse momentum $k_\perp$. The so-called Boer-Mulders function $h_{1,\pi}^\perp(x,\boldsymbol{k}_\perp^2)$ [7,34] describes a spin-orbit correlation of transversely polarized partons, which is chirally and ("naively") time-reversal odd. "Chirally odd" means that the operator structure defining $h_{1,\pi}^\perp(x,\boldsymbol{k}_\perp^2)$ flips the chirality of the partons, implying that this function can enter the description of a process only in combination with another chiral-odd function. "Time-reversal odd" (T-odd) means that under time-reversal transformations the correlation flips sign, while the Wilson lines inherent in the TMD operator definitions are transformed from future to past pointing or vice versa. This implies that T-odd functions appear with different signs in deep-inelastic scattering (DIS) and DY process [35–41]. The different signs of T-odd TMDs in different processes can be tested experimentally in the case of the nucleon, though this is not feasible for the pion.

However, the T-odd correlations as described by the Boer-Mulders functions in the pion and nucleon may be responsible for the violation of the Lam-Tung relation, which connects the coefficients in the angular distribution of the DY lepton pairs [42–44]. The π-nucleus DY data [13–15] show a significant violation of this relation, which calls for a nonperturbative leading-twist mechanism beyond collinear factorization. The Boer-Mulders effect provides such a mechanism within the TMD factorization framework [34], though alternative mechanisms have also been proposed [45–49]. Indications for the violation of the Lam-Tung relation were also observed in pp- and pd-induced DY [50].

In order to perform the nonperturbative calculations of the pion TMDs $f_{1,\pi}(x,\boldsymbol{k}_\perp^2)$ and $h_{1,\pi}^\perp(x,\boldsymbol{k}_\perp^2)$ we use the light-front formalism, where hadrons are described in terms of light-front wave functions (LFWFs). The latter are expressed as an expansion of various quark, antiquark and gluon Fock components. In principle, there is an infinite number of LFWFs in such an expansion. However, there are many situations where one can successfully model hadronic wave functions by confining oneself to the contribution of the minimal Fock-space configuration with a few partons. We will refer to this approach as the light-front constituent model (LFCM). The LFCM was successfully applied to describe many nucleon properties

[51–60] including TMDs [61–64]. For the pion, the specific model we will adopt for the minimal Fock-space components of the LFWF has been originally proposed in Refs. [65,66], and has been applied to study some partonic properties of the pion in Refs. [67,68]. However, the present work is the first application to study the TMDs in the pion.

The description of nucleon TMDs within the LFCM was shown to agree with phenomenology within (10–30)% in the valence-x region after evolution from the low initial scale of the model to experimentally relevant scales [62,64]. This is in particular the case for the Boer-Mulders function of the nucleon [64].

In this work we derive and calculate the unpolarized TMD and Boer-Mulders function of the pion, $f_{1,\pi}(x,\boldsymbol{k}_\perp^2)$ and $h_{1,\pi}^\perp(x,\boldsymbol{k}_\perp^2)$, and compute the coefficient ν in π-nucleus induced DY. We find that the valence distribution function $f_{1,\pi}(x)$ of the pion obtained from the LFCM agrees well with available parametrizations. We compare our results for the pion Boer-Mulder function with previous results from spectator and bag models Refs. [69–72] as well as with lattice QCD [73]. We show that $h_{1,\pi}^\perp(x,\boldsymbol{k}_\perp^2)$, in combination with the nucleon Boer-Mulders function $h_{1,N}^\perp(x,\boldsymbol{k}_\perp^2)$ from the LFCM of Ref. [63], gives a good description of the DY data on the coefficient ν. For other model studies of the nucleon Boer-Mulders function and phenomenological work related to the violation of the Lam-Tung relation we refer to Refs. [34,74–86].

The outline of this work is as follows. In Sec. II we determine the initial scale of the pion LFCM approach. In Sec. III we review the classification of the pion LFWF, in the minimal $(q\bar{q})$ Fock-space configuration, in terms of light-front amplitudes describing the different $\bar{q}q$ orbital angular-momentum components in the pion state. In Sec. IV we derive the representation of the leading-twist pion TMDs as overlap of light-front amplitudes. In Sec. V we use a specific model for the pion LFWFs to obtain numerical results for pion TMDs at the initial hadronic scale. We then evolve and discuss our results. Section VI gives a brief review of the DY formalism at a leading-order parton-model level. Section VII is dedicated to a discussion of the unpolarized TMD in the DY process, and establishes the range of applicability of our approach. In Sec. VIII we discuss the Boer-Mulders effect in π-nucleus induced DY. Finally, in Sec. IX we summarize our results and give an outlook.

II. INITIAL SCALE OF THE PION CONSTITUENT APPROACH

Parton distribution functions are defined within a certain regularization scheme at a given renormalization scale. The results from a constituent approach refer to an assumed low initial scale μ_0, at which a pion is thought to consist of a "valence" quark-antiquark pair only, while a nucleon is similarly assumed to consist of three valence quarks only. The value of μ_0 is not known *a priori*, but it can be determined in a way independent of the details of the constituent model. Therefore we shall first address this point, before embarking with the actual study of TMDs in LFCM.

It is crucial to determine μ_0 for two reasons. First, the model parton distributions have to be evolved from a well-defined initial scale μ_0 to experimentally relevant scales $Q \sim$ few GeV before they can be confronted with data. Second, the initial scale μ_0 determines the value of the running coupling constant $\alpha_s(\mu_0^2)$ which enters the overall normalization of the Boer-Mulders function, when the initial (final) state interaction effects are taken into account via the one-gluon-exchange mechanism (see the discussion in Sec. IV B).

To determine μ_0 we use the following standard procedure [53,87–89]. At the initial scale the entire pion momentum must be carried by valence $\bar{q}$, q degrees of freedom, $\langle x\rangle_v = 1$, while sea-quark and gluon contributions are set to zero. Similar to Ref. [87] we then require the initial scale μ_0 to be such that after evolution from μ_0 to say $Q^2 = 4$ GeV^2 the phenomenological value for the pion momentum fraction carried by valence quarks is reproduced. We take

$$\langle x\rangle_v = \int_0^1 \mathrm{d}x x[(f^u_{1,\pi^+} - f^{\bar{u}}_{1,\pi^+})(x) + (f^{\bar{d}}_{1,\pi^+} - f^d_{1,\pi^+})(x)] = 0.47 \pm 0.02 \quad \text{at } Q^2 = 4 \text{ GeV}^2 \tag{1}$$

in leading order (LO) and next-to-leading order (NLO) from the parametrizations [90,91]. We use $\alpha_{\rm LO}(M_Z^2) = 0.13939$ and $\alpha_{\rm NLO}(M_Z^2) = 0.12018$ in $\overline{\rm MS}$ scheme for the strong coupling constant at the Z_0 mass $M_Z = 91.1$ GeV from the global fit of parton distribution functions (PDFs) to hard-scattering data from Ref. [92]. These values correspond to $\Lambda_{\rm LO} = 359,\ 322,\ 255$ MeV and $\Lambda_{\rm NLO} = 402,\ 341,\ 239$ MeV for respectively $N_F = 3, 4, 5$ flavors in the variable flavor-number scheme with heavy-quark mass thresholds at $m_c = 1.4$ GeV, $m_b = 4.75$ GeV, $m_t = 175$ GeV [92].

With these parameters the above described procedure yields at LO and NLO for the initial scale

$$\mu_{0,\rm LO} = 460 \text{ MeV}, \qquad \frac{\alpha_{\rm LO}(\mu_0^2)}{4\pi} = 0.225, \tag{2}$$

$$\mu_{0,\rm NLO} = 555 \text{ MeV}, \qquad \frac{\alpha_{\rm NLO}(\mu_0^2)}{4\pi} = 0.0938. \tag{3}$$

In a different NLO scheme the numerical values in Eq. (3) would be somewhat different, but it is beyond the scope of this work to study scheme-dependence effects. In the following we shall assume that theoretical uncertainties due to scheme dependence are smaller than the generic accuracy of (light-front) constituent model approaches.

At this point it is instructive to compare the LO and NLO initial scales for pion distribution functions, Eqs. (2) and (3), with those obtained in the case of the nucleon [64]. In principle, the constituent model approaches for the pion and nucleon can be viewed as unrelated models. Nevertheless, the underlying physical assumption is the same. At some low "hadronic scale" one deals with constituent (valence) degrees of freedom carrying the total hadron momentum: a constituent quark-antiquark pair in the pion case, or three constituent quarks in the nucleon case. For the underlying physical picture to be successful one should expect the initial scale to be "universal," i.e. independent of the considered hadron. It is therefore gratifying to observe how close numerically the results are for the nucleon case (in [64] it was obtained $\mu_{0,\mathrm{LO}} = 420$ MeV and $\mu_{0,\mathrm{NLO}} = 508$ MeV for the nucleon) as compared to the pion case in Eqs. (2) and (3). This is an encouraging indication for the usefulness of the constituent model picture.

III. LIGHT-FRONT AMPLITUDES IN THE PION CONSTITUENT APPROACH

In this section, we review the classification of the light-front wave function for the pion, considering the minimal Fock-space configuration, i.e. $q\bar{q}$. According to the total quark orbital angular-momentum projection, the $q\bar{q}$ LFWF of the pion can be written in terms of two light-front amplitudes carrying the total quark orbital angular momentum $l_z = 0$ and $|l_z| = 1$, i.e.

$$|\pi(p)\rangle_{q\bar{q}} = |\pi(p)\rangle_{q\bar{q}}^{l_z=0} + |\pi(p)\rangle_{q\bar{q}}^{|l_z|=1}. \tag{4}$$

The different angular-momentum components of the state in Eq. (4) are given by [93,94]

$$|\pi(p)\rangle_{q\bar{q}}^{l_z=0} = T_\pi \int \mathrm{d}[1]\mathrm{d}[2]\psi^{(1)}(1,2)\frac{\delta_{ij}}{\sqrt{3}}[q^\dagger_{i\uparrow}(1)\bar{q}^\dagger_{j\downarrow}(2) - q^\dagger_{i\downarrow}(1)\bar{q}^\dagger_{j\uparrow}(2)]|0\rangle, \tag{5}$$

$$|\pi(p)\rangle_{q\bar{q}}^{|l_z|=1} = T_\pi \int \mathrm{d}[1]\mathrm{d}[2]\psi^{(2)}(1,2)\frac{\delta_{ij}}{\sqrt{3}}[k^-_{1\perp}q^\dagger_{i\uparrow}(1)\bar{q}^\dagger_{j\uparrow}(2) + k^+_{1\perp}q^\dagger_{i\downarrow}(1)\bar{q}^\dagger_{j\downarrow}(2)]|0\rangle, \tag{6}$$

where $k^\pm_{i\perp} = k^x_i \pm k^y_i$, and $q^\dagger_{i\lambda}$ and $\bar{q}^\dagger_{i\lambda}$ are creation operators of a quark and antiquark with flavor q, helicity λ and color i, respectively. In Eqs. (5) and (6), T_π is the isospin factor which projects on the different members of the isotriplet of the pion, and is defined as $T_\pi = \sum_{\tau_q\tau_{\bar{q}}}\langle 1/2\tau_q 1/2\tau_{\bar{q}}|1\tau_\pi\rangle$ with $\tau_q, \tau_{\bar{q}}$ and τ_π the isospin of the quark, antiquark and pion state, respectively. Furthermore, the amplitudes $\psi^{(1,2)}(1,2)$ are functions of quark momenta with arguments 1 representing x_1 and $\boldsymbol{k}_{1\perp}$ and so on. They depend on the transverse momenta only through scalar products, e.g. $\boldsymbol{k}_{i\perp}\cdot\boldsymbol{k}_{j\perp}$. Since momentum conservation implies $\boldsymbol{k}_{1\perp} + \boldsymbol{k}_{2\perp} = 0$ and $x_1 + x_2 = 1$, $\psi^{(1,2)}_{q\bar{q}}(1,2)$ depend only on the variables $\bar{x} = x_1$ and $\boldsymbol{\kappa}^2_\perp$, with $\boldsymbol{\kappa}_\perp = \boldsymbol{k}_{1\perp}$. The integration measure in Eqs. (5) and (6) is defined as

$$\mathrm{d}[1]\mathrm{d}[2] = \frac{\mathrm{d}x_1\mathrm{d}x_2}{\sqrt{x_1x_2}}\delta\left(1 - \sum_{i=1}^{2}x_i\right)\frac{\mathrm{d}^2\boldsymbol{k}_{1\perp}\mathrm{d}^2\boldsymbol{k}_{2\perp}}{[2(2\pi^3)]}\delta^2\left(\sum_{i=1}^{2}\boldsymbol{k}_{i\perp}\right) = \frac{\mathrm{d}\bar{x}}{\sqrt{\bar{x}(1-\bar{x})}}\frac{\mathrm{d}^2\boldsymbol{\kappa}_\perp}{[2(2\pi^3)]}. \tag{7}$$

In the following, we will describe the above LFWF amplitudes in a light-front constituent model which was already successfully applied for describing the charge form factor and decay constant of the pion [65,66] and the generalized parton distributions [67,68].

The $q\bar{q}$ component of the light-front state of the pion can be written as

$$|\pi(p)\rangle_{q\bar{q}} = T_\pi\sum_{\lambda_i,c_i}\int \mathrm{d}[1]\mathrm{d}[2]\Psi^{[f]}_{q\bar{q}}(\{x_i,\boldsymbol{k}_{i\perp};\lambda_i\})\frac{\delta_{ij}}{\sqrt{3}}q^\dagger_{i\lambda_1}(1)\bar{q}^\dagger_{j\lambda_2}(2)|0\rangle. \tag{8}$$

In Eq. (8), the LFWF $\Psi^{[f]}_{q\bar{q}}(\{x_i,\boldsymbol{k}_{i\perp};\lambda_i\})$ satisfies Poincaré covariance and is an eigenstate of the total angular-momentum operator in the light-front dynamics. These properties can be fulfilled by constructing the wave function as the product of a momentum wave function, which is spherically symmetric and invariant under permutation of the two constituent partons, and a spin wave function, which is uniquely determined by symmetry requirements, i.e.,

$$\Psi^{[f]}_{q\bar{q}}(\{x_i,\boldsymbol{k}_{i\perp};\lambda_i\}) = \tilde{\psi}_\pi(\bar{x},\boldsymbol{\kappa}_\perp)\tilde{\Phi}(\lambda_1,\lambda_2). \tag{9}$$

In the above equation, the spin-dependent part is given by

$$\tilde{\Phi}(\lambda_1,\lambda_2)=\sum_{\mu_1\mu_2}\langle 1/2,\mu_1;1/2,\mu_2|0,0\rangle D^{1/2*}_{\mu_1\lambda_1}(R_M(\boldsymbol{\kappa}))D^{1/2*}_{\mu_2\lambda_2}(R_M(-\boldsymbol{\kappa})), \tag{10}$$

where $\boldsymbol{\kappa}=\{\boldsymbol{\kappa}_\perp,\kappa_z\}$, with

$$\kappa_z=M_0(\bar{x},\boldsymbol{\kappa}_\perp)\left(\bar{x}-\frac{1}{2}\right), \tag{11}$$

and the free mass defined as

$$M_0^2(\bar{x},\boldsymbol{\kappa}_\perp)=\frac{m^2+|\boldsymbol{\kappa}_\perp|^2}{\bar{x}(1-\bar{x})}, \tag{12}$$

with m the quark mass. In Eq. (10), $D^{1/2}_{\lambda\mu}(R_M(\bar{x},\boldsymbol{\kappa}_\perp))$ is the matrix element of the Melosh rotation R_M [95]

$$D^{1/2}_{\lambda\mu}(R_M(\boldsymbol{\kappa}))=\langle\lambda|R_M(\boldsymbol{\kappa})|\mu\rangle = \left\langle\lambda\left|\frac{m+\bar{x}M_0-i\boldsymbol{\sigma}\cdot(\hat{\boldsymbol{z}}\times\boldsymbol{\kappa}_\perp)}{\sqrt{(m+\bar{x}M_0)^2+\boldsymbol{\kappa}_\perp^2}}\right|\mu\right\rangle. \tag{13}$$

The Melosh rotation corresponds to the unitary transformation which converts the Pauli spinors of the quark and antiquark in the pion rest frame to the light-front spinor. Making explicit the dependence on the quark and antiquark helicities, the spin wave function of Eq. (10) takes the following values:

$$\tilde{\Phi}(\uparrow,\uparrow)=\prod_i\frac{1}{\sqrt{N(x_i,\boldsymbol{\kappa}_\perp)}}\kappa_\perp^-(-a_1+a_2), \tag{14}$$

$$\tilde{\Phi}(\uparrow,\downarrow)=\prod_i\frac{1}{\sqrt{N(x_i,\boldsymbol{\kappa}_\perp)}}(a_1a_2-\kappa_\perp^+\kappa_\perp^-), \tag{15}$$

$$\tilde{\Phi}(\downarrow,\uparrow)=\prod_i\frac{1}{\sqrt{N(x_i,\boldsymbol{\kappa}_\perp)}}(-a_1a_2+\kappa_\perp^+\kappa_\perp^-), \tag{16}$$

$$\tilde{\Phi}_\uparrow(\downarrow,\downarrow)=\prod_i\frac{1}{\sqrt{N(x_i,\boldsymbol{\kappa}_\perp)}}\kappa_\perp^+(-a_1-a_2), \tag{17}$$

where $a_i=(m+x_iM_0)$, and $N(x_i,\boldsymbol{\kappa}_\perp)=[(m+x_iM_0)^2+\boldsymbol{\kappa}_\perp^2]$. Taking into account the quark-helicity dependence in Eqs. (14)–(17), the pion state can be mapped out into the different angular-momentum components. As a result, the pion wave function amplitudes in the LFCM read

$$\psi^{(1)}(1,2)=\tilde{\psi}(x,\boldsymbol{\kappa}_\perp)\prod_i\frac{1}{\sqrt{N(x_i,\boldsymbol{\kappa}_\perp)}}\frac{1}{\sqrt{2}}(a_1a_2-\kappa_\perp^-\kappa_\perp^+), \tag{18}$$

$$\psi^{(2)}(1,2)=\tilde{\psi}(x,\boldsymbol{\kappa}_\perp)\prod_i\frac{1}{\sqrt{N(x_i,\boldsymbol{\kappa}_\perp)}}\frac{1}{\sqrt{2}}(-a_1-a_2). \tag{19}$$

IV. TWIST-2 TMDS IN THE PION CONSTITUENT APPROACH

The quark TMDs are defined through the following correlation function [6–8]

$$\Phi_{ij}(x,\boldsymbol{k}_\perp^2)=\int\frac{d\xi^-d^2\boldsymbol{\xi}_\perp}{(2\pi)^3}e^{ik\cdot\xi}\langle p|\bar{\psi}_j(0)\mathcal{L}^\dagger(0,\boldsymbol{0}_\perp|n)\mathcal{L}(\xi^-,\boldsymbol{\xi}_\perp|n)\psi_i(\xi)|p\rangle|_{\xi^+=0}, \tag{20}$$

where $x=k^+/p^+$ and for a generic four-vector $a^\mu=(a^+,a^-,\boldsymbol{a}_\perp)$ we used the light-front components $a^\pm=(a^0\pm a^3)/\sqrt{2}$. The Wilson lines $\mathcal{L}$ connecting the two quark fields ensure the color gauge invariance of the correlator in Eq. (20) and are defined as [6–8]

$$\mathcal{L}(\xi^-,\boldsymbol{\xi}_\perp|n)=\mathcal{P}\exp\left(-ig\int_{\xi^-}^{n\cdot\infty}d\eta^-\cdot A^+(\eta^-,\boldsymbol{\xi}_\perp)\right)\mathcal{P}\exp\left(-ig\int_{\boldsymbol{\xi}_\perp}^{\infty}d^2\boldsymbol{\eta}_\perp\cdot\boldsymbol{A}_\perp(\xi^-=n\cdot\infty,\boldsymbol{\eta}_\perp)\right), \tag{21}$$

where the vector n depends on the process under consideration. For instance, the future-pointing Wilson lines with $n=(0,+1,0)$ are appropriate for defining TMDs in semi-inclusive DIS (SIDIS), whereas in the Drell-Yan process the Wilson lines are necessarily past pointing with $n=(0,-1,0)$. In particular, this reverses the sign of all T-odd distribution functions entering the correlator.

For a pion target, the information content of the correlator (20) is summarized at leading twist by two TMDs that can be projected out from the correlator as follows:

$$\frac{1}{2}\mathrm{Tr}[\Phi\gamma^+] = f_{1,\pi}(x,\boldsymbol{k}_\perp^2), \tag{22}$$

$$\frac{1}{2}\mathrm{Tr}[\Phi i\sigma^{i+}\gamma_5] = \frac{\epsilon^{ij}k_\perp^j}{M_\pi} h_{1,\pi}^\perp(x,\boldsymbol{k}_\perp^2). \tag{23}$$

The function $f_{1,\pi}(x,\boldsymbol{k}_\perp^2)$ is the unpolarized quark distribution, which integrated over $\boldsymbol{k}_\perp$ gives the familiar parton momentum distribution $f_{1,\pi}(x)$ (in the parton model; in the TMD factorization framework the relation is more subtle [3]), and $h_{1,\pi}^\perp(x,\boldsymbol{k}_\perp^2)$ is the Boer-Mulders TMD [7], which is a T-odd function, i.e. it changes sign under "naive time reversal" defined as usual time reversal, but without interchange of initial and final states. In the following, we will present the model calculation of the Boer-Mulders function for the SIDIS process denoted as $h_{1,\pi}^\perp(x,\boldsymbol{k}_\perp^2)_{\mathrm{DIS}}$, while for the Boer-Mulders function in the Drell-Yan process we will use $h_{1\pi}^\perp(x,\boldsymbol{k}_\perp^2)_{\mathrm{DY}} = -h_{1,\pi}^\perp(x,\boldsymbol{k}_\perp^2)_{\mathrm{DIS}}$.

A. Unpolarized parton distribution function in the pion

From the definition (22), the $f_{1,\pi}$ TMD to leading order in the gauge field is given by

$$f_{1,\pi}(x,\boldsymbol{k}_\perp^2) = \int \frac{\mathrm{d}\xi^-\mathrm{d}^2\boldsymbol{\xi}_\perp}{(2\pi)^3} e^{i(\xi^- k^+ - \boldsymbol{\xi}_\perp\cdot\boldsymbol{k}_\perp)} \langle\pi(p)|\bar\psi(0)\gamma^+\psi(\xi^-,\boldsymbol{\xi}_\perp)|\pi(p)\rangle. \tag{24}$$

By using the canonical expansion of the quark fields in terms of Fock operators and taking into account the $q\bar q$ component of the light-front state of the pion in Eq. (8), we find the final result

$$\begin{aligned} f_{1,\pi}^q(x,\boldsymbol{k}_\perp^2) = f_{1,\pi}^{\bar q}(x,\boldsymbol{k}_\perp^2) &= T_\pi^2 \int \mathrm{d}[1]\mathrm{d}[2]\sqrt{x_1x_2}\,\delta(x-x_1)\delta^2(\boldsymbol{k}_\perp - \boldsymbol{k}_{1\perp})|\tilde\psi_\pi(x_1,\boldsymbol{k}_{\perp 1})|^2 \\ &= T_\pi^2 \frac{1}{2(2\pi)^3}|\tilde\psi_\pi(x,\boldsymbol{k}_\perp)|^2. \end{aligned} \tag{25}$$

The unpolarized TMD involves a matrix element which is diagonal in the quark orbital angular momentum. As a consequence, it takes the following expression in terms of the wave function amplitudes in Eqs. (5) and (6):

$$f_{1,\pi}^q(x,\boldsymbol{k}_\perp^2) = T_\pi^2 \frac{1}{(2\pi)^3}[|\tilde\psi^{(1)}(x,\boldsymbol{k}_\perp^2)|^2 + \boldsymbol{k}_\perp^2|\tilde\psi^{(2)}(x,\boldsymbol{k}_\perp^2)|^2]. \tag{26}$$

B. Boer-Mulders function of the pion

Using the definitions (20) and (23), the quark Boer-Mulders function of the pion is given by

$$h_{1,\pi}^\perp(x,\boldsymbol{k}_\perp^2)_{\mathrm{DIS}} = \epsilon^{ij}k^j\frac{M_\pi}{2\boldsymbol{k}_\perp^2}\int \frac{\mathrm{d}\xi^-\mathrm{d}^2\boldsymbol{\xi}_\perp}{(2\pi)^3} e^{i(\xi^- k^+ - \boldsymbol{\xi}_\perp\cdot\boldsymbol{k}_\perp)} \langle\pi(p)|\bar\psi(0)\mathcal{L}^\dagger(0,\boldsymbol{0}_\perp|n)i\sigma^{i+}\gamma_5\mathcal{L}(\xi^-,\boldsymbol{\xi}_\perp|n)\psi(\xi^-,\boldsymbol{\xi}_\perp)|\pi(p)\rangle, \tag{27}$$

with $n = (0,+1,0)$. The gauge link $\mathcal{L}$ is crucial to obtain a nonzero Boer-Mulders function. In the light-front gauge, it reduces to a transverse gauge link at $\xi^- = \infty$ given by the second term in Eq. (21). Furthermore, we expand the above gauge link to take into account the first order nonvanishing contribution corresponding to the one-gluon-exchange diagram shown in Fig. 1. Following the procedure outlined in Ref. [63] for the analogous calculation of the T-odd TMDs of the nucleon, we obtain the following result for the quark Boer-Mulders function of the pion

$$\begin{aligned} h_{1,\pi}^{\perp q}(x,\boldsymbol{k}_\perp^2)_{\mathrm{DIS}} = -g^2M_\pi\frac{k_\perp^x - ik_\perp^y}{\boldsymbol{k}_\perp^2}\frac{1}{(2\pi)^{11}}\frac{1}{\sqrt{2k^+}}\int\frac{\mathrm{d}k_3^+\mathrm{d}^2\boldsymbol{k}_{3\perp}}{\sqrt{(2k_3^+)(2k_4^+)}}\int\frac{\mathrm{d}^2\boldsymbol{q}_\perp}{2k_1^+} \\ \times\left\{\frac{1}{\boldsymbol{q}_\perp^2}\sum_{\lambda_3}\sum_{\bar q}\sum_{i,j}\sum_{k,l}T_{ij}^aT_{kl}^b\delta_{ab}\langle\pi(p)|q_{i\uparrow}^\dagger(k_1)q_{j\downarrow}(k)\bar q_{k\lambda_3}(k_4)\bar q_{l\lambda_3}^\dagger(k_3)|\pi(p)\rangle\right\}, \end{aligned} \tag{28}$$

where the parton momenta are defined as $k_1 = k - q$, $k_4 = k_3 - q$. The above equation corresponds to the diagram of Fig. 1 with $\lambda = -\lambda_1$ and $\lambda_4 = \lambda_3$ for the helicity of the interacting and spectator partons, respectively, i.e. the helicity is conserved at the antiquark-gluon vertex, while the helicity of the struck quark flips from the initial to the final state. For angular-momentum conservation, the quark-helicity flip must be compensated by a transfer of one unit of orbital angular

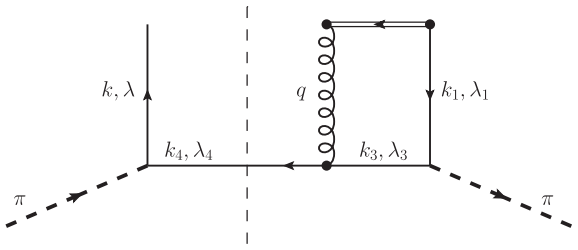

+ H.c.

FIG. 1. The leading contribution from the one-gluon-exchange mechanism to the T-odd distribution function of the pion.

momentum. Inserting in Eq. (28) the LFWF amplitude decomposition of the pion state introduced in Sec. III, one finds the following results in terms of the light-front amplitudes $\psi^{(i)}$

$$h_{1,\pi}^{\perp q}(x,\boldsymbol{k}_\perp^2)_{\rm DIS} = \frac{4}{3} g^2 T_\pi^2 M_\pi \frac{k_\perp^x - i k_\perp^y}{\boldsymbol{k}_\perp^2} \int \frac{\mathrm{d}^2\boldsymbol{q}_\perp}{(2\pi)^5} \frac{1}{\boldsymbol{q}_\perp^2} \mathcal{H}_\pi^{\perp q}, \quad (29)$$

where the function $\mathcal{H}_\pi^{\perp q}$ is

$$\mathcal{H}_\pi^{\perp q} = -k_\perp'^{+} \psi^{(1)}(1,2)\psi^{(2)*}(1',2') + k_\perp^{+} \psi^{(1)*}(1,2)\psi^{(2)}(1',2') \quad (30)$$

with $\boldsymbol{k}'_\perp = \boldsymbol{k}_\perp - \boldsymbol{q}_\perp$ and the parton coordinates $1 = (x, \boldsymbol{k}_\perp)$, $2 = (1-x, -\boldsymbol{k}_\perp)$, and $1' = (x, \boldsymbol{k}'_\perp)$, $2' = (1-x, -\boldsymbol{k}'_\perp)$. In the model for the light-front amplitudes introduced in Sec. III, we find the following explicit results

$$h_{1,\pi}^{\perp q}(x,\boldsymbol{k}_\perp^2)_{\rm DIS} = \frac{4}{3} g^2 T_\pi^2 M_\pi \frac{k_\perp^x - i k_\perp^y}{\boldsymbol{k}_\perp^2} \int \frac{\mathrm{d}^2\boldsymbol{q}_\perp}{(2\pi)^5} \frac{1}{\boldsymbol{q}_\perp^2} \tilde{\psi}^*(\{x_i'\},\{\boldsymbol{k}'_{i\perp}\}) \tilde{\psi}(\{x_i\},\{\boldsymbol{k}_{i\perp}\}) \times \frac{1}{2} \prod_{i=1}^{2} N^{-1}(\boldsymbol{k}_i') N^{-1}(\boldsymbol{k}_i) [\tilde{A}_1 A_2 + \tilde{\boldsymbol{B}}_1 \cdot \boldsymbol{B}_2], \quad (31)$$

where we introduced the definitions

$$\begin{aligned}
\tilde{A}_1 &= (m + x_1 M_0)(k_1'^x + i k_1'^y) - (m + x_1' M_0')(k_1^x + i k_1^y),\\
\tilde{B}_1^x &= -i(m + x_1' M_0')(m + x_1 M_0) + i(k_1'^x + i k_1'^y)(k_1^x + i k_1^y),\\
\tilde{B}_1^y &= (m + x_1' M_0')(m + x_1 M_0) + (k'_{1,x} + i k'_{1y})(k_1^x + i k_1^y),\\
\tilde{B}_1^z &= i(m + x_1' M_0')(k_1^x + i k_1^y) + i(m + x_1 M_0)(k_1'^x + i k_1'^y),
\end{aligned} \quad (32)$$

for the contribution from the active quark, and

$$\begin{aligned}
A_2 &= (m + x_2 M_0)(m + x_2' M_0') + k_2^x k_2'^x + k_2^y k_2'^y,\\
B_2^x &= -(m + x_2' M_0') k_2^x + (m + x_2 M_0) k_2'^y,\\
B_2^y &= (m + x_2' M_0') k_2^x - (m + x_2 M_0) k_2'^x,\\
B_2^z &= k_2'^x k_2^y - k_2'^y k_2^x,
\end{aligned} \quad (33)$$

for the contribution of the spectator antiquark.

The Boer-Mulders function for the valence antiquark can be obtained through a similar calculation by replacing the antiquark spectator with the quark spectator. As a result, one finds $h_{1,\pi}^{\perp \bar{q}} = h_{1,\pi}^{\perp q}$.

V. RESULTS FROM A LIGHT-FRONT CONSTITUENT MODEL

Up to this point we made only general assumptions. We have chosen to work in a constituent approach of the pion, and determined its initial scale in Sec. II. We have then chosen to use the light-front formalism and presented in Sec. III a general discussion of light-front amplitudes in the pion constituent approach. In Sec. IV we derived a model-independent representation of the leading-twist pion TMDs as overlap of light-front amplitudes for the $q\bar{q}$ Fock state of the pion. In this section we will apply the formalism from Secs. III and IV to obtain predictions for pion TMDs using a specific model for the momentum-dependent part of the LFWF.

A. Model for the momentum-dependent wave function

The formalism described in the previous sections is applied to a specific choice for the LFCM, namely the model proposed in Refs. [65,66]. The model is specified by adopting the following exponential form for the momentum-dependent part of the pion wave function

$$\tilde{\psi}_\pi(\bar{x}, \boldsymbol{\kappa}_\perp) = [2(2\pi)^3]^{1/2} \left(\frac{M_0(\bar{x}, \boldsymbol{\kappa}_\perp)}{4\bar{x}(1-\bar{x})} \right)^{1/2} \times \frac{1}{\pi^{3/4} \beta^{3/2}} \exp\left(-\boldsymbol{\kappa}^2/(2\beta^2)\right). \quad (34)$$

The wave function in Eq. (34) is normalized as

$$\int_0^1 \mathrm{d}\bar{x} \int \frac{\mathrm{d}\boldsymbol{\kappa}_\perp}{2(2\pi)^3} |\tilde{\psi}_\pi(\bar{x}, \boldsymbol{\kappa}_\perp)|^2 = 1$$

[recalling that $\mathrm{d}\kappa_z = \mathrm{d}\bar{x}\ M_0(\bar{x}, \boldsymbol{\kappa}_\perp)/[4\bar{x}(1-\bar{x})]$], and depends on the free parameter β and the quark mass m, which have been fitted to the pion charge radius and decay constant. In particular, we take $m = 0.250$ GeV and

$\beta = 0.3194$ [65]. As we are considering only the leading $q\bar{q}$ Fock-space component in the pion LFWF, the quark (antiquark) contribution to the pion distribution functions at the hadronic scale of the model coincides with the valence quark q_v (antiquark $\bar{q}_v$) contribution, while the sea-quark contribution is vanishing. Furthermore, isospin symmetry imposes $j^{u_v}_{\pi^+} = j^{\bar{d}_v}_{\pi^+} = j^{d_v}_{\pi^-} = j^{\bar{u}_v}_{\pi^-} = \frac{1}{2} j^{u_v}_{\pi^0} = \frac{1}{2} j^{\bar{u}_v}_{\pi^0} = \frac{1}{2} j^{d_v}_{\pi^0} = \frac{1}{2} j^{\bar{d}_v}_{\pi^0}$, with $j = f_1, h_1^\perp$. In the following, we will refer to distributions of valence quarks and antiquarks in charged pions, using the notation $j^{q_v}_\pi$ and $j^{\bar{q}_v}_\pi$, respectively.

B. Results for $f^{q_v}_{1,\pi}(x, k_\perp^2)$ at the hadronic scale

In Fig. 2, we show the model predictions for the valence-quark contribution to the unpolarized TMD as a function of x and $\boldsymbol{k}_\perp^2$. The results refer to the low hadronic scale determined in Sec. II. For the $q\bar{q}$ component of the pion state, the distribution of a quark with longitudinal momentum fraction x is equal to the distribution of an antiquark with longitudinal momentum fraction $1-x$, i.e. $f^{q_v}_{1,\pi}(x, \boldsymbol{k}_\perp^2) = f^{\bar{q}_v}_{1,\pi}(1-x, \boldsymbol{k}_\perp^2)$. Furthermore, one has the relation $f^{q_v}_{1,\pi}(x, \boldsymbol{k}_\perp^2) = f^{\bar{q}_v}_{1,\pi}(x, \boldsymbol{k}_\perp^2)$, which gives as a final result a momentum distribution symmetric with respect to $x = 1/2$. We also observe a rapid falloff with $\boldsymbol{k}_\perp^2$, with a decreasing slope at larger x. This behavior can be better seen in Fig. 2(b) where we plot the $f^{u_v}_{1,\pi}$ TMD as a function of $\boldsymbol{k}_\perp^2$ at different values of x. We notice that the $\boldsymbol{k}_\perp^2$ dependence is definitely not Gaussian, but it can be approximated by a Gaussian function with reasonable accuracy. Upon integration over $\boldsymbol{k}_\perp$, we obtain the unpolarized PDF. In Fig. 2(c) we compare the unpolarized quark distribution of the pion $f_{1,\pi}(x)$ with the results of the unpolarized quark distribution of the proton $f_{1,p}(x)$ obtained from the three-quark LFWF of Ref. [61]. The shape of the distributions for the pion and proton is quite different, reflecting the different valence-quark structure of the hadrons. For the proton, the momentum distribution of the valence quark is peaked at $x \approx 1/3$. Moreover, the SU(6) symmetry for the spin-flavor structure of the LFWF in [61] gives $f^{u_v}_{1,p}(x) = 2 f^{d_v}_{1,p}(x)$.

C. Evolved results for $f^{q_v}_{1,\pi}(x)$ in comparison to parametrizations

As a first test of the applicability of the LFCM to the description of partonic properties of the pion, we compare the results for $f^{u_v}_{1,\pi}(x)$ evolved from the initial scale of the model to $Q^2 = 25$ GeV^2, with available parametrizations [90,91,96–100] (for a review of the pion PDF in the valence-x region see also Ref. [101]). The initial-scale, LO-evolved and NLO-evolved distributions are shown in Fig. 3(a). The LO and NLO evolutions are applied starting from the initial scales $\mu^2_{0,\mathrm{LO}}$ and $\mu^2_{0,\mathrm{NLO}}$ in Eqs. (2) and (3), respectively. Remarkably, although the initial scales and especially the values of $\alpha_s(\mu_0^2)$ at LO and NLO differ, the evolved results are numerically close. This kind of behavior has been interpreted in Refs. [90,96,102,103] as an indication for the "convergence" of perturbation theory down to low scales.

It is important to keep in mind that the LO and NLO parametrizations of [90,96,102] differ slightly at their respective low scales, such that they allow one to describe data equally well in the combination with the LO or NLO hard parts in the respective LO or NLO treatments. In contrast, our model input at the initial scale is identical in LO and NLO. This inevitably introduces a scheme dependence, when applying the model results beyond LO. But we feel that such scheme-dependence effects are smaller than the generic model accuracy, as discussed in Sec. II. Considering that in the context of parton structure studies the generic model accuracy is observed to be around (10–30)% [62], we interpret the result in Fig. 3(a), i.e.

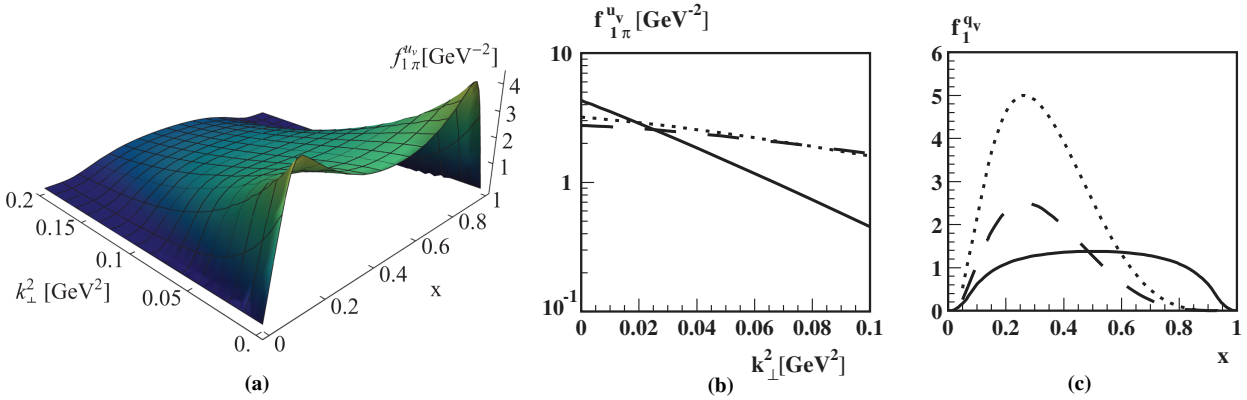

FIG. 2 (color online). The valence-quark unpolarized TMD of the pion from the LFWF (34) at the hadronic scale. (a) $f^{u_v}_{1,\pi^+}(x, \boldsymbol{k}_\perp^2)$ as a function of x and $\boldsymbol{k}_\perp^2$. (b) $f^{u_v}_{1,\pi}$ as a function of $\boldsymbol{k}_\perp^2$ for selected values of x ($x = 0.1$ solid curve, $x = 0.3$ dotted curve, $x = 0.5$ dashed curve). (c) Comparison of the unpolarized PDFs as functions of x in the pion and nucleon from LFCM approaches at their initial hadronic scales. Solid line: $f^{u_v}_{1,\pi}(x)$ in the pion obtained in this work. Dotted (dashed) curve: $f^{u_v}_{1p}(x)$ [$f^{d_v}_{1p}(x)$] in the proton from the light-front constituent quark model of Ref. [61].

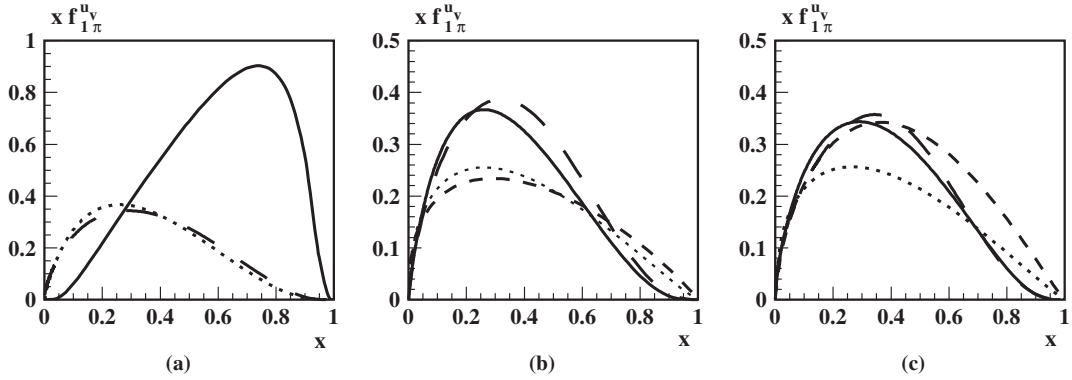

FIG. 3. (a) $xf^{u_v}_{1,\pi}(x)$ as function of x. Solid line: at initial scale of the model. Dotted line: LO evolved to 25 GeV^2. Dashed line: NLO evolved to 25 GeV^2. (b) $xf^{u_v}_{1,\pi}(x)$ as function of x after LO evolution to $Q^2 = 25$ GeV^2 in comparison to the LO parametrizations from [97] (dashed curve) and [96] (dotted curve), and the calculation of [98] (long-dashed curve). (c) $xf^{u_v}_{1,\pi}(x)$ as function of x after NLO evolution to $Q^2 = 25$ GeV^2 in comparison to the NLO parametrizations from [99] (long-dashed curve), [91] (dashed curve) and [90,96] (dotted curve).

the "convergence" of the LO and NLO results in the sense of Refs. [90,96,102,103], as an indication that the issue of applicability of perturbative evolution equations down to the low scales in Eqs. (2) and (3) is not the dominant source of theoretical uncertainty in our approach.

In Fig. 3(b) the LFCM results at LO are compared with the LO parametrizations of Refs. [96,97] and the calculation using Dyson-Schwinger equations of Ref. [98]. In Fig. 3(c) we compare our NLO results with the NLO phenomenological fits of Refs. [90,91,96] and the results from the recent analysis of Ref. [99]. The evolution effects are important, and change the shape of the distribution by leading to the convex-up behavior near $x = 1$, typical of the renormalization group equations which populate the sea-quark distribution at small x at the expense of the large-x valence-quark contribution. In particular, the LFCM results are in good agreement with the recent analysis of Ref. [99] and the calculation [98] showing a falloff at large x much softer than the linear behavior obtained from the other analysis.

We remark that there is a recent extraction [100] of the pion PDF in the valence region obtained from an updated NLO analysis of the Fermilab pion DY data. These results are consistent with the parametrization of Ref. [90] in the valence-x region and therefore we do not show them explicitly in Fig. 3(c). In summary, we observe that the partonic description of the pion works with the same level of accuracy observed for the LFCM of the nucleon [62].

D. Results for the Boer-Mulders function at low initial scale

Having convinced ourselves that the pion LFCM provides a reasonable description of the unpolarized TMD, we now focus on what this approach predicts for the Boer-Mulders function.

The overall normalization of the Boer-Mulders function contains (in leading order of the Wilson line expansion) the parameter g^2 in Eqs. (28), (29) and (31). At first glance it may appear natural to associate g^2 with the strong coupling at the low initial scale, $\alpha(\mu_0^2) = g^2/(4\pi)$, and eventually we shall do this. But it is worth discussing this choice in some more detail, because in a nonperturbative calculation this is a nontrivial step which should be done with care. The expansion of the Wilson line is certainly appropriate for demonstrating "matters of principle" such as the existence of T-odd TMDs in QCD [35,36]. But it is *a priori* not clear whether this approach provides an adequate description of nonperturbative hadronic physics. From this point of view, one could consider the one-gluon-exchange approximation as an effective description. Besides the pioneering efforts of Ref. [71], nothing is known about effects from the Wilson line beyond one-gluon exchange. One could therefore understand g^2 as a free parameter and choose its value to "effectively" account for higher order effects, which would be understood as part of the model. For instance, the value of g^2 could be adjusted to reproduce data. While in principle perfectly legitimate, we feel that here this would be an impractical procedure.

In the context of the pion Boer-Mulders function not much data are available, and at the present state of the art the analysis of that data bears uncertainties which are difficult to control. We therefore prefer not to introduce a free parameter at this point. Instead we fix $\alpha(\mu^2_{0,\mathrm{NLO}}) = g^2/(4\pi)$ in Eq. (3). One could have also chosen to reproduce the LO value $\alpha(\mu^2_{0,\mathrm{LO}})$ in Eq. (2). However, the choice of NLO value $\alpha(\mu^2_{0,\mathrm{NLO}})$ is preferable over the LO value $\alpha(\mu^2_{0,\mathrm{LO}})$ for two reasons. First, the NLO value can be associated with higher stability from the perspective of perturbative convergence [53,87–89], and may be interpreted as effectively considering higher order effects in the above explained sense. Second, a smaller value of $\alpha(\mu^2_{0,\mathrm{NLO}})$ helps to better comply with positivity constraints (see below). However, let us stress that fixing the value of g^2 in the overall normalization of the Boer-Mulders

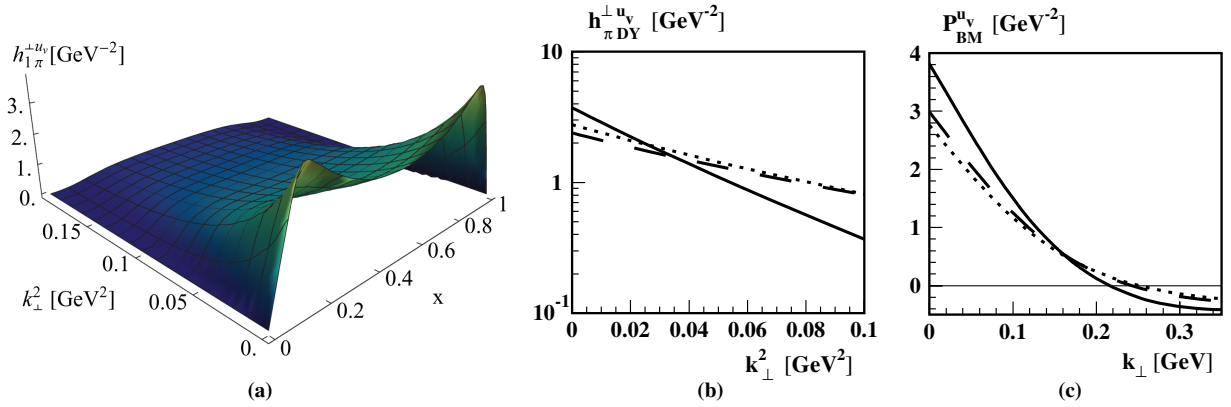

FIG. 4 (color online). The Boer-Mulder function of the pion in the DY process from the LFCM at initial scale. (a) $h_{1,\pi}^{\perp u_v}(x,\boldsymbol{k}_\perp^2)$ as a function of x and $\boldsymbol{k}_\perp^2$. (b) $h_{1,\pi}^{\perp u_v}$ as a function of $\boldsymbol{k}_\perp^2$ for selected values of x ($x = 0.1$ solid curve, $x = 0.3$ dotted curve, $x = 0.5$ dashed curve). (c) The positivity relation (32) for the valence-u quark in the pion as a function of $k_\perp$ at different values of x: $x = 0.2$ (solid curve), $x = 0.35$ (dashed curve) and $x = 0.5$ (dotted curve).

function is part of the modeling, and one could revisit this choice, if it gave unsatisfactory phenomenological results. Below we shall see that our choice leads to satisfactory results.

In Fig. 4(a) we show the LFCM results for the Boer-Mulders TMD as function of x and $\boldsymbol{k}_\perp^2$ with the sign as it is expected to appear in the DY process. The shape of the distribution is very similar to the unpolarized TMD. It is symmetric with respect to $x = 1/2$, with a peak at $x \sim 0.1$, and is rapidly decreasing at larger $\boldsymbol{k}_\perp^2$, with a falloff which is not Gaussian but can be approximated reasonably well by a Gaussian function. This is evident from Fig. 4(b) which displays the $\boldsymbol{k}_\perp^2$ dependence at selected values of x. The slope in $\boldsymbol{k}_\perp^2$ of the Boer-Mulders function is slightly steeper than that of the unpolarized TMD, in particular at larger values of x.

The next important test of the model calculation is posed by positivity [104] which requires that in the pion the unpolarized and Boer-Mulders TMD obey the following positivity relation, which holds flavor by flavor,

$$P_{\rm BM}^q(x,\boldsymbol{k}_\perp^2) \equiv f_{1,\pi}^q(x,\boldsymbol{k}_\perp^2) - \frac{k_\perp}{M_\pi}|h_{1,\pi}^{\perp q}(x,\boldsymbol{k}_\perp^2)| \geq 0. \quad (35)$$

The model results for $P_{\rm BM}^q(x,\boldsymbol{k}_\perp^2)$ at selected values of x are plotted in Fig. 4(c).[1] We see that the inequality (32) is safely satisfied for $k_\perp \lesssim 0.2$ GeV but violated for larger $k_\perp$. Calculations in effective nonperturbative model frameworks may provide some insights into the properties of TMDs for $k_\perp \ll \mu_0$, but the description of the region $k_\perp \sim \mathcal{O}(\mu_0)$ is out of scope. Nevertheless, from the point of view of internal consistency, the noncompliance with (35) at large $k_\perp$ is of course unsatisfactory. This happens, to the best of our knowledge, also in all presently available calculations of T-odd TMDs [105]. The general reasons for that can be traced back to an inconsistent treatment: T-odd TMDs are calculated to "first order of the expansion of the Wilson line," whereas T-even TMDs like $f_1^q(x,\boldsymbol{k}_\perp^2)$ are evaluated to "zeroth order" in that expansion. To preserve positivity the Wilson link expansion should be truncated consistently at the same order for both T-odd and T-even TMDs which enter the inequality (35) on the same footing [64].

From the point of view of practical applications, it is gratifying to observe that the inequality (35) is violated only in the region of small x or large $k_\perp$ [64,105], i.e. in a region of parameter space that is beyond the range of applicability of effective quark models. In particular, we convinced ourselves here that in the LFCM of the pion the noncompliance with inequalities in the extreme regions of the $(x,k_\perp)$ space has no practical consequences for the description of physical processes, provided one uses the model within its range of applicability. The same observation was made in the case of the description of nucleon T-odd TMDs in the constituent quark model framework [64].

E. Comparison to results for Boer-Mulders functions from different models

It is instructive to compare the Boer-Mulders functions of a pion and nucleon. Let us define the $(1/2)$- and (1)-transverse moments of the pion and proton Boer-Mulders functions as

$$h_{1,h}^{\perp(1/2)}(x) = \int \mathrm{d}^2\boldsymbol{k}_\perp \frac{k_\perp}{2M_h} h_{1,h}^\perp(x,\boldsymbol{k}_\perp^2),$$
$$h_{1,h}^{\perp(1)}(x) = \int \mathrm{d}^2\boldsymbol{k}_\perp \frac{\boldsymbol{k}_\perp^2}{2M_h^2} h_{1,h}^\perp(x,\boldsymbol{k}_\perp^2). \quad (36)$$

[1]We remark that if both functions had exactly Gaussian $k_\perp$ behavior (which they have not), the steeper $\boldsymbol{k}_\perp^2$ slopes of $h_{1,\pi}^{\perp q}(x,\boldsymbol{k}_\perp^2)$ observed in Fig. 4(b) as compared to $f_{1,\pi}^q(x,\boldsymbol{k}_\perp^2)$ in Fig. 2(b) would be a necessary (though not sufficient) condition to satisfy positivity.

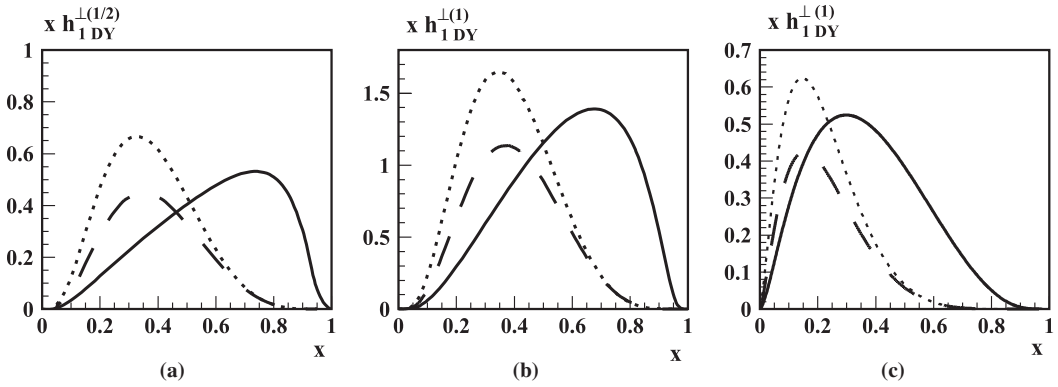

FIG. 5. (a) Comparison of $xh_1^{\perp(1/2)q_v}(x)$ in the DY process as functions of x in the pion and nucleon from LFCM approaches at initial scales. Solid line: u_v distribution in the pion, this work. Dotted (dashed) curve: u_v (d_v) distribution in the proton, Ref. [61]. (b) The results for $xh_{1\mathrm{DY}}^{\perp(1)}$ as a function of x . Solid curve: u_v distribution in the pion. Dotted (dashed) curve: u_v (d_v) distribution in the proton, from the LFCM of Ref. [64]. The proton results are rescaled by a factor M_p/M_π. (c) The same as in Fig. 5(b) but at $Q^2 = 25$ GeV^2 obtained with approximate LO evolution from the LFCM results at the hadronic scale.

Owing to the appearance of hadron masses in the correlators defining the Boer-Mulders functions in Eq. (23), the magnitude of the (1) moment of the pion Boer-Mulders function is artificially enhanced by a factor $\sim M_p/M_\pi$ with respect to the nucleon case. Therefore, in the following plots, we will rescale the results for the (1) moment of the proton Boer-Mulders function by that factor, in such a way that the comparison with the results for the pion is not distorted by the numerically very different values of pion and nucleon masses.

Figure 5(a) compares the results for $h_{1,\pi}^{\perp(1/2)u_v}(x)$ obtained here and $h_{1,p}^{\perp(1/2)q_v}(x)$ obtained in [64]. Similarly, Fig. 5(b) shows the results for the (1) moment of the pion Boer-Mulders function in comparison with the corresponding results for valence quarks in the proton rescaled by a factor M_p/M_π. In both cases, the distributions for the valence contribution in the proton and pion have comparable magnitude, but similar to the case of the unpolarized PDF, the x dependence is quite different. The sign of the pion Boer-Mulders function is consistent with the sign of the Boer-Mulders function of the proton [70], as obtained also in lattice calculations [73], the MIT bag model [72] and spectator models [71,75]. Interestingly, in comparison with other model calculations like the spectator model [71,75] and MIT bag model [72], the shape and the magnitude of $h_{1,\pi}^{\perp}$ from LFCM are quite different. Similar differences have been found also in the comparison of the model results for the proton Boer-Mulders function [63,64]. The LFCM predictions for the nucleon Boer-Mulders function favorably describe available SIDIS data [64]. In Sec. VIII we will see that the LFCM predictions for the pion Boer-Mulders function provide a similarly satisfactory description of DY data.

F. Estimating the x evolution for the Boer-Mulders function

For phenomenological applications we will need the pion Boer-Mulders function from the LFCM evolved to experimentally relevant scales. This requires both, evolution in x and transverse momentum. In this section we discuss the x evolution (the evolution of the transverse momentum dependence will be discussed in the next section.)

Recently, substantial progress on the evolution of TMDs has been achieved [3,28–32]. However, the exact evolution equations for the Boer-Mulders function are still under study. At the present stage we have to resort to approximations in order take into account effects of scale dependence. To this aim, we will follow the same strategy as we adopted for the Boer-Mulders function of the proton [64], and approximate the evolution of transverse moments of the Boer-Mulders function by using the evolution equations of the chiral-odd transversity distribution function in the nucleon (in a spin-zero hadron, like the pion, there is of course no transversity distribution, but the pion Boer-Mulders originates from the same unintegrated chiral-odd correlator).

To be more precise, we will evolve the (1) moments of the Boer-Mulders functions. Such transverse moments appear naturally in transverse momentum weighted azimuthal asymmetries, and it was argued that asymmetries weighted in this way are less affected by Sudakov effects [106]. It will be possible to ultimately judge the quality of this approximation only after the exact evolution equations are known. But we feel confident that the uncertainty introduced by this step in our theoretical study is not larger than the generic accuracy of the LFCM.

Figure 5(c) show the results for (1) moment $xh_{1\mathrm{DY}}^{\perp(1)}$ after approximate (transversity) LO evolution from the initial scale in Eq. (2) to $Q^2 = 25$ GeV^2. For comparison we include also the results for the nucleon Boer-Mulders functions rescaled by a factor M_p/M_π. As in the case of the unpolarized PDF, the effects of the evolution are sizable, producing a shift of the peak position towards smaller x and reducing the magnitude of the distribution.

In Sec. VI we will use the model predictions to describe azimuthal asymmetries in DY in a LO treatment. For this

purpose, we will use the results for $f_{1,\pi}(x)$ and $h_{1,\pi}^{\perp(1)}(x)$ LO evolved in x to experimental scales—exactly and approximately, respectively, as described in Sec. V C and the present Sec. V F. Before applying the model results to phenomenology, in the following section we will estimate the broadening of transverse momenta at the large scales typically probed in DY experiments.

VI. THE DRELL-YAN PROCESS WITH UNPOLARIZED HADRONS

In this section we introduce the concepts required to describe the Drell-Yan process in the parton model taking into account transverse momentum effects. Our treatment will be pragmatic and phenomenological.

A. Kinematics, variables, conventions

Let $p_{1,2}$ denote the momenta of the incoming hadrons $h_{1,2}$, and let l, l' be the momenta of the outgoing lepton pair. The kinematics of the process is described by the center-of-mass energy square s, invariant mass of the lepton pair Q, rapidity y or the Feynman variable x_F, and the variable τ which are defined and related to each other as

$$\begin{aligned} &s = (p_1 + p_2)^2, \qquad q = l + l', \qquad Q^2 = q^2, \\ &y = \frac{1}{2}\ln\frac{p_2\cdot q}{p_1\cdot q} = \frac{1}{2}\ln\frac{x_1}{x_2}, \qquad x_F = x_1 - x_2, \\ &\tau \equiv \frac{Q^2}{s} = x_1 x_2. \end{aligned} \tag{37}$$

In the parton model the x_i denote the fractions of the hadron momenta p_i carried by (respectively) the annihilating parton or antiparton, and are given by (the $+$ signs refer to x_1, the $-$ signs x_2)

$$x_{1,2} = \pm\frac{x_F}{2} + \sqrt{\frac{x_F^2}{4} + \tau} = \sqrt{\tau}e^{\pm y}. \tag{38}$$

In the lab frame, where one hadron is a target or where both hadrons are beam particles, the produced lepton pair will in general have a three-momentum $\boldsymbol{q} = \boldsymbol{l} + \boldsymbol{l}' \neq 0$. It is often convenient to analyze the data in a dilepton rest frame. There are various frames, including several dilepton rest frames, that are routinely used for data analyses, see Refs. [18–22] for an overview. The differences between the different frames are of order $\mathcal{O}(q_T/Q)$. In the following we will work in the Collins-Soper frame, which is defined in Fig. 6, and use only data analyzed in that frame.

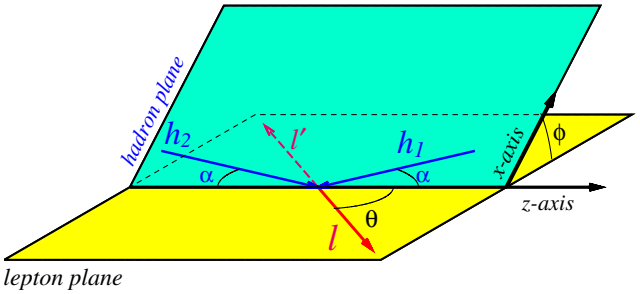

FIG. 6 (color online). The definition of the angles θ and ϕ in the Collins-Soper frame. This frame is the center-of-mass frame of the produced leptons in which the hadrons are incoming symmetrically with respect to the z axis (at an angle α in the figure) with the transverse momentum q_T.

In this work we will consider pion-nucleus collisions. The used convention is such that x_1 describes the momentum fraction of the parton from π^-, while x_2 describes the momentum fraction of the parton from the nucleon bound in the nucleus. In order to describe nuclei with proton number Z and neutron number N we will neglect nuclear binding effects and assume that, for instance, $f^u_{1/\text{ nucleus}} = (Z/A)f^u_{1/\text{ proton}} + (N/A)f^u_{1/\text{ neutron}}$, where $A = N + Z$ denotes the mass number of the nucleus. The neglect of nuclear binding effects is a justified step for $q_T \lesssim 3$ GeV [14,16], which includes the kinematic region of interest for our study.

B. Structure functions in unpolarized DY

The angular distribution of the DY lepton pairs originating from collisions of unpolarized hadrons is given in the Collins-Soper frame by (see Fig. 6 for the definition of angles),

$$\frac{\mathrm{d}N}{\mathrm{d}\Omega} \equiv \frac{\mathrm{d}\sigma}{\mathrm{d}^4q\mathrm{d}\Omega} \Big/ \frac{\mathrm{d}\sigma}{\mathrm{d}^4q} = \frac{3}{4\pi}\frac{1}{\lambda+3}\left(1 + \lambda\cos^2\theta + \mu\sin 2\theta\cos\phi + \frac{\nu}{2}\sin^2\theta\cos 2\phi\right). \tag{39}$$

In the notation of Ref. [20] the coefficients λ, μ, ν can be expressed in terms of DY structure functions as follows:

$$\lambda = \frac{F^1_{UU} - F^2_{UU}}{F^1_{UU} + F^2_{UU}}, \quad \mu = \frac{F^{\cos\phi}_{UU}}{F^1_{UU} + F^2_{UU}}, \quad \nu = \frac{2F^{\cos 2\phi}_{UU}}{F^1_{UU} + F^2_{UU}}. \tag{40}$$

The so-called Lam-Tung relation claims $\lambda + 2\nu = 1$, which reads in terms of structure functions $F^2_{UU} = 2F^{\cos 2\phi}_{UU}$. This relation is exact if one treats the DY process to $\mathcal{O}(\alpha_s)$ in the standard collinear factorization QCD framework [42,43]. At $\mathcal{O}(\alpha_s^2)$ the Lam-Tung relation is violated, though at a numerically negligible rate [44]. However, DY data from pion-nucleus collisions show that it is strongly violated, calling for a nonperturbative

leading-twist mechanism beyond collinear factorization. The Boer-Mulders effect provides such a mechanism [34]. Alternative nonperturbative mechanisms to explain this observation have been proposed in [45–49].

C. Parton-model treatment

In a tree-level parton-model approach including transverse parton momenta in the region $q_T \ll Q$ the structure functions F_{UU}^1 and $F_{UU}^{\cos 2\phi}$ are leading twist, $F_{UU}^{\cos\phi}$ is subleading twist, and F_{UU}^2 is a power-suppressed higher-twist effect proportional to q_T^2/Q^2. In such a treatment the transverse dilepton momenta q_T arise from the convolutions of ("intrinsic") transverse momenta of the partons as described through TMDs. The leading-twist structure functions in the unpolarized DY process are expressed in terms of TMDs through the following convolution integrals [20]

$$F_{UU}^1(x_1,x_2,q_T) = \frac{1}{N_c}\sum_a e_a^2 \int \mathrm{d}^2\boldsymbol{k}_{1\perp}\mathrm{d}^2\boldsymbol{k}_{2\perp}\delta^{(2)}(\boldsymbol{q}_T-\boldsymbol{k}_{1\perp}-\boldsymbol{k}_{2\perp}) f_{1,\pi}^a(x_1,\boldsymbol{k}_{1\perp}^2) f_{1,N}^{\bar a}(x_2,\boldsymbol{k}_{2\perp}^2), \tag{41}$$

$$F_{UU}^{\cos(2\phi)}(x_1,x_2,q_T) = \frac{1}{N_c}\sum_a e_a^2 \int \mathrm{d}^2\boldsymbol{k}_{1\perp}\mathrm{d}^2\boldsymbol{k}_{2\perp}\delta^{(2)}(\boldsymbol{q}_T-\boldsymbol{k}_{1\perp}-\boldsymbol{k}_{2\perp})\omega_{\mathrm{BM}} h_{1,\pi}^{\perp a}(x_1,\boldsymbol{k}_{1\perp}^2)_{\mathrm{DY}} h_{1,N}^{\perp \bar a}(x_2,\boldsymbol{k}_{2\perp}^2)_{\mathrm{DY}},$$
$$\omega_{\mathrm{BM}} = \frac{2(\boldsymbol{q}_T\cdot\boldsymbol{k}_{1\perp})(\boldsymbol{q}_T\cdot\boldsymbol{k}_{2\perp}) - q_T^2(\boldsymbol{k}_{1\perp}\cdot\boldsymbol{k}_{2\perp})}{M_\pi M_N q_T^2}, \tag{42}$$

where the sums go over $a = u, \bar u, d, \bar d$, and, in principle, heavier flavors.

At this point it is important to recall that the parton-model description is adequate and works reasonably well for some observables, but not for all. For instance, in order to describe absolute cross sections (even if averaged over transverse dilepton momenta), it is necessary to go to the NLO QCD treatment of the process. We will work in a LO ("tree-level") formalism and consider ratios of cross sections where "overall normalizations" tend to cancel out. Indeed, experience in various processes shows that different types of corrections may significantly affect absolute cross sections, but tend to cancel in cross section ratios. To quote just a few examples, we mention in this context the weak scale dependence of longitudinal spin asymmetries in DIS [107], or the near cancellation of resummation effects of large double logarithmic QCD corrections in longitudinal spin asymmetries in SIDIS [108]. In longitudinal and transverse spin asymmetries in DY higher order QCD corrections also tend to cancel [109–111], and the same tendency is found for partonic threshold corrections [112]. QCD corrections to polarization effects in e^+e^- annihilation tend also to cancel [113]. This is encouraging, but of course does not prove that higher order corrections will tend to cancel also for the cross section ratios considered in this work, and more theoretical work is needed to attest this point. We finally remark, that our parton-model treatment does not consider the color entanglement effects discussed in Ref. [114].

VII. THE UNPOLARIZED TMDS IN DY

The LFCM was shown to describe the x dependence of $f_{1,h}$ with an accuracy of (10–30)% within the range of applicability of the model. (For the pion see Sec. V, for the nucleon see Ref. [60].) In this section we will therefore focus entirely on the $k_\perp$ dependence.

A. Gaussian approximation and estimate of $k_\perp$ broadening for $f_{1,h}^a(x,\boldsymbol{k}_\perp^2)$

The LFCM predictions for the $k_\perp$ dependence of TMDs presented in Sec. V refer to a low scale of ~0.5 GeV, and cannot be applied directly to describe DY data which are typically taken in the region $Q \sim$ (4–9) GeV between the J/ψ and Υ resonances, or above the Υ resonance region. In order to estimate the $k_\perp$-evolution effects we shall resort to the Gaussian ansatz, and proceed phenomenologically. The procedure is motivated and outlined below.

The DY cross section behaves like $\mathrm{d}\sigma/\mathrm{d}q_T^2 \propto \exp(-q_T^2/\langle q_T^2\rangle)$ for $q_T \ll Q$ [115–117]. This observation is the basis for the popularity of the Gaussian ansatz to model the distributions of transverse parton momenta in hadrons. Although certainly oversimplifying, the phenomenological success of the Gaussian ansatz indicates that it is a useful working assumption. We shall therefore recast the model predictions for TMD as follows:

$$f_{1,h}^a(x,\boldsymbol{k}_\perp^2) = f_{1,h}^a(x)\frac{\exp(-\boldsymbol{k}_\perp^2/\langle k_{\perp,\mathrm{unp}}^{2a/h}(x)\rangle)}{\pi\langle k_{\perp,\mathrm{unp}}^{2a/h}(x)\rangle},$$
$$\langle k_{\perp,\mathrm{unp}}^{2a/h}(x)\rangle = \frac{\int \mathrm{d}^2\boldsymbol{k}_\perp \boldsymbol{k}_\perp^2 f_{1,h}^a(x,\boldsymbol{k}_\perp^2)}{\int \mathrm{d}^2\boldsymbol{k}_\perp f_{1,h}^a(x,\boldsymbol{k}_\perp^2)}, \tag{43}$$

where $f_{1,h}^a(x)$ is the unpolarized collinear parton distribution function.

Before describing in detail how we estimate $k_\perp$-evolution effects, let us comment on a feature concerning Eq. (43). In Sec. V we have seen that the model results for pion TMDs exhibit an approximate Gaussian behavior. The

same was demonstrated in [62,64] for the nucleon case. In contrast to Refs. [62,64] (where predictions from the LFCM of the nucleon were applied to SIDIS phenomenology) in this work we do not take the Gaussian widths to be x-independent constants. Rather, in Eq. (43) we allow a more flexible parametrization with x-dependent Gaussian widths. This has the advantage of further improving the quality of the Gaussian approximation.

The exact evolution of the $k_\perp$ dependence of the unpolarized TMD is known in the Collins-Soper-Sterman (CSS) formalism, which provides a framework for a quantitative description of transverse momentum broadening effects with increasing energies. The underlying physical picture is that with increasing energy gluon radiation broadens the "initial" (or "intrinsic") parton transverse momentum. There is no practical or theoretical way to separate "nonperturbative intrinsic" and "perturbative gluon-radiation" effects. However, from a phenomenological point of view, there is no need for that: both effects are collectively parametrized in the effective parameters in Eq. (43), provided one pays due attention to apply this effective description to the region of low transverse momenta $q_T \ll Q$ [116,117]. In order to estimate this effective broadening of the Gaussian widths we shall use the results from [117].

In principle one could directly work within the CSS formalism. However, the CSS formalism has not yet been established for the Boer-Mulders effect. Moreover, even in the unpolarized case, it has not yet been studied whether one can use the CSS formalism starting from a scale as low as in Eqs. (2) and (3). In this work we therefore prefer to use the effective description of [117] to estimate $k_\perp$-evolution effects, which requires us to use the Gaussian ansatz, as done in Eq. (43). The details of this step will be described below.

Let us now turn our attention to the description of the transverse parton momenta in DY. We discuss first the mean transverse momenta of the produced lepton pairs [see Eqs. (37) and (38) for the relation of x_F with $x_{1,2}$] defined as

$$\langle q_T^2(x_F,s)\rangle = \frac{\int \mathrm{d}^2 q_T q_T^2 F^1_{UU}(x_1,x_2,q_T)}{\int \mathrm{d}^2 q_T F^1_{UU}(x_1,x_2,q_T)}. \tag{44}$$

It is important to notice that in a LO formalism the energy (or scale) dependence is introduced by using parton distributions (LO) evolved to the relevant scale, and using appropriately broadened Gaussian widths. We also notice that $\langle q_T^2(x_F,s)\rangle$ is a ratio of observables, i.e. amenable to the description in a parton-model approach thanks to the approximate cancellation of higher order QCD effects, as argued in Sec. VI C.

When using the Gaussian ansatz in a tree-level parton-model approach, the $\langle q_T^2\rangle$ is given by the sum of the Gaussian widths of the unpolarized TMDs of the nucleon and pion. (In general this would hold only if the Gaussian widths were flavor independent. In the LFCM, where sea quarks are absent, it also holds because only one flavor contributes to the production of the lepton pair, namely a valence $\bar{u}$ from the π^- and a valence u in the proton annihilate.)

If we used the model results discussed in Sec. V at their face value to estimate $\langle q_T^2\rangle$ we would strongly underestimate the data. This is not surprising as the model results have to be evolved. In order to estimate evolution effects, we add an energy-dependent constant $\langle \delta k_\perp^2(s)\rangle$ such that

$$\langle q_T^2(x_F,s)\rangle = \langle k^{2\bar{u}/\pi^-}_{\perp,\mathrm{unp}}(x_1)\rangle + \langle k^{2u/N}_{\perp,\mathrm{unp}}(x_2)\rangle + \langle \delta k^2_{\perp,\ \mathrm{unp}}(s)\rangle. \tag{45}$$

The energy dependence of $\langle q_T^2\rangle$ enters only through $\langle \delta k^2_{\perp,\ \mathrm{unp}}(s)\rangle$ which provides the amount of transverse momentum broadening at given s. The variation of dilepton momenta with s was investigated phenomenologically in [115,117]. These studies allow us to estimate the amount of $k_\perp$ broadening required in our approach to be

$$\langle \delta k^2_{\perp,\ \mathrm{unp}}(s)\rangle = \delta A_{\mathrm{unp}} + B_{\mathrm{unp}} s, \qquad \delta A_{\mathrm{unp}} = 0.4\ \mathrm{GeV}^2, \qquad B_{\mathrm{unp}} = 2.6\times 10^{-3}. \tag{46}$$

It is important to stress that $\langle \delta k^2_{\perp,\mathrm{unp}}(s)\rangle$ constitutes the accumulated $k_\perp$ broadening in both the pion and nucleon. Notice that $\langle \delta k^2_{\perp,\mathrm{unp}}(s)\rangle$ could also depend on x_F or other variables besides s, but we disregard this possibility here. Finally, one should stress that the linear broadening indicated in (46) is valid only in a narrow s range [115,117]. When considering broader energy ranges up to collider energies the increase is $\log s$ [118] rather than linear.

B. Comparison to the data

With the empirical estimate of $k_\perp$-broadening effects in Sec. VII A, the model results yield a good description of DY data in the region $s \sim (50\text{–}600)\ \mathrm{GeV}^2$ studied in Refs. [115,117]. We present two examples to illustrate this.

Figure 7 shows how our approach describes Fermilab E615 data on $\langle q_T^2(x_F)\rangle$ of Drell-Yan lepton pairs produced in collisions of 80 and 252 GeV π^- beams impinging on tungsten targets [12,15], which corresponds respectively to $s \simeq 150$ and 473 GeV^2. We obtain a good description of the 80 GeV data [12] in the region $0.2 \le x_F \lesssim 0.8$. The 252 GeV data are well described for $0 \le x_F \lesssim 0.5$. Considering the generic accuracy $\sim$(10–30)% of the LFCM, the description of these data in the region $0.5 \lesssim x_F \lesssim 0.7$ can be still considered satisfactory. However, beyond $x_F \gtrsim 0.7$ the approach breaks down. This is not a failure of the model (which admittedly is not applicable at small or large x), but of the TMD approach in general. The reason is as follows. At large x_F the breakdown of the description of the DY process in terms of parton

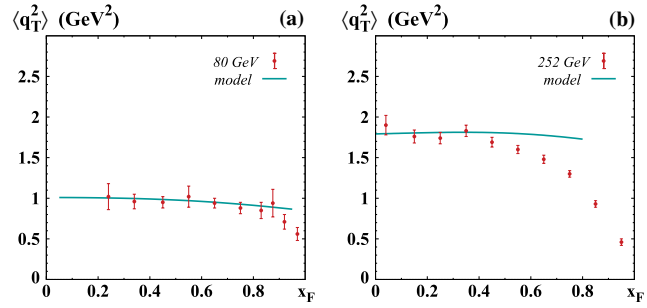

FIG. 7 (color online). The mean dimuon transverse momentum square $\langle q_T^2 \rangle$ vs x_F from the Fermilab E615 experiment taken with respectively (a) 80 GeV [12] and (b) 252 GeV [15] π^- beams impinging on tungsten targets. The theoretical curves are the result from LFCM obtained in this work with a phenomenological estimate for transverse momentum broadening, see Eqs. (45) and (46).

distribution functions is expected. The limit $x_F \to 1$ corresponds to large x_1 in the pion (and small x_2 in the nucleon). As $x_1 \to 1$ the $\bar{u}$ from the π^- is far off shell, and more appropriately described in terms of the pion distribution amplitude [119]. While this so-called Berger-Brodsky effect provides a unique opportunity to access information on the pion distribution amplitude [120], from the point of view of the TMD description of the DY process it is a power correction, which dominates as one approaches the limit $x_F \to 1$ of the available phase space. Interestingly the Gaussian ansatz itself still works even for $x_F \gtrsim 0.7$ [117]. In principle one could continue using the TMD description, at least in some parts of the large-x_F region. This would require narrower $\langle q_T^2(x_F) \rangle$. The x_F dependence of $\langle q_T^2(x_F) \rangle$ implied by the LFCM through the x dependence of the Gaussian widths in Eq. (43) is not sufficient for that, but one could introduce an adequate x_F dependence of the transverse momentum broadening $\langle \delta k_{\perp,\mathrm{unp}}^2(s) \rangle$ in addition to its s dependence. In this work we shall refrain from such attempts, stick to our x_F-independent description of transverse momentum broadening in Eqs. (45) and (46), and keep in mind that this description has limitations at large x_F.

The observable $\langle q_T^2(x_F) \rangle$ shown in Fig. 7 is the result of averaging over DY pair momenta. It is of importance to demonstrate that our approach works also for observables depending on q_T. For that we consider the data from the E615 experiment [15] shown in Fig. 8 on the normalized cross sections, which we define for brevity as

$$\frac{1}{\sigma}\frac{\mathrm{d}\sigma(q_T)}{\mathrm{d}q_T} \equiv \frac{\mathrm{d}^2\sigma(q_T, x_F)}{\mathrm{d}q_T \mathrm{d}x_F} \Big/ \frac{\mathrm{d}\sigma(x_F)}{\mathrm{d}x_F} = \frac{2\pi q_T \langle F_{UU}^1(x_1, x_2, q_T) \rangle}{\langle F_{UU}^1(x_1, x_2) \rangle}, \tag{47}$$

where $\langle \cdots \rangle$ denote averages over x_F in certain bins, and σ in the first term of Eq. (47) is a shortcut notation for the differential cross section $\mathrm{d}\sigma/\mathrm{d}x_F$. The normalization is such that one obtains unity after integrating over q_T in Eq. (47). Using the Gaussian ansatz, the structure functions are given by

$$F_{UU}^1(x_1, x_2, q_T) = \frac{1}{N_c} \sum_a e_a^2 f_{1,\pi}^a(x_1) f_{1,N}^{\bar{a}}(x_2) \frac{\exp(-q_T^2/\langle q_T^2 \rangle)}{\pi \langle q_T^2 \rangle}, \tag{48}$$

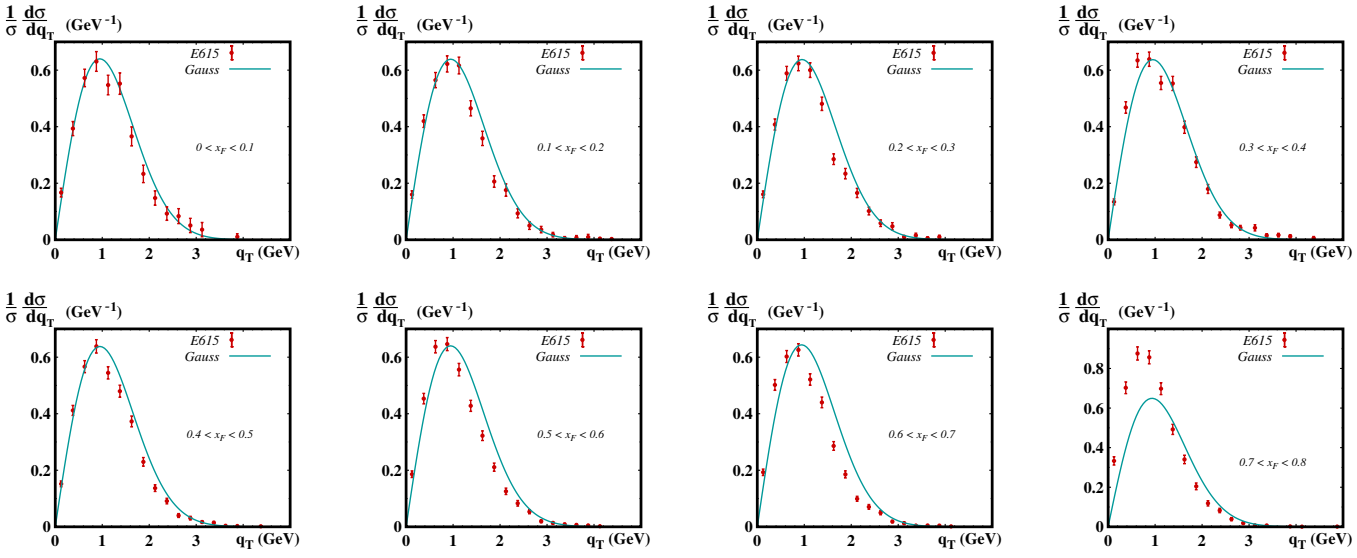

FIG. 8 (color online). The normalized cross section $(1/\sigma)(\mathrm{d}\sigma(q_T)/\mathrm{d}q_T)$ as functions of q_T in different x_F bins. The data are from Ref. [15]. The theoretical curves are from the LFCM with transverse momentum broadening effects estimated according to Eqs. (45) and (46). The description of the data is very good in the region $0 \le x_F \le 0.5$, and it is still acceptable for $0.5 \le x_F \lesssim 0.7$. For $x_F \gtrsim 0.7$ the description breaks down, because the TMD approach is not applicable and higher twist effects become relevant.

$$F^1_{UU}(x_1,x_2)=\frac{1}{N_c}\sum_a e_a^2 f^a_{1,\pi}(x_1)f^{\bar a}_{1,N}(x_2). \quad (49)$$

Notice that $F^1_{UU}(x_1,x_2,q_T)$ in Eq. (48) depends on the Gaussian model, but after integrating out transverse momenta one obtains the model-independent structure function $F^1_{UU}(x_1,x_2)=\int \mathrm{d}^2q_T F^1_{UU}(x_1,x_2,q_T)$ in Eq. (49). The data refer to $4.05\le Q/\mathrm{GeV}\le 8.55$ and were taken with a 252 GeV π^- beam impinging on a nuclear (tungsten) target [15]. Thus $s\simeq 473\ \mathrm{GeV}^2$ in this experiment. Strictly speaking we could only retrieve E615 data on $\mathrm{d}^2\sigma/(\mathrm{d}q_T\mathrm{d}x_F)$ from Ref. [17], and estimated the differential cross sections $\mathrm{d}\sigma/\mathrm{d}x_F$ ourselves, to obtain the normalized data in Fig. 8. We are confident that the data shown in Fig. 8 are normalized with an accuracy of 10%, which is comparable or better than the accuracy of the LFCM. [We recall that we work in a LO approach. Thus, we could have alternatively studied the q_T dependence of the differential cross sections $\mathrm{d}^2\sigma/(\mathrm{d}q_T\mathrm{d}x_F)$ fixing the overall normalizations "by hand," or estimating "K factors." Both alternatives are not more rigorous than our treatment.]

Figure 8 shows that the description of the q_T dependence of the normalized cross sections works very well in the region $0\le x_F\le 0.5$, and is still reasonably good for $0.5\le x_F\lesssim 0.7$, but for $x_F\gtrsim 0.7$ it clearly breaks down, which is not surprising given our earlier findings concluded from Fig. 7 and the expectations from QCD for $x_F\to 1$ [119]. It is important to stress that we do not only expect limitations of the approach at large x_F, but in particular also at large q_T, where the Gaussian ansatz is at variance with QCD which predicts a powerlike decay [121]. These limitations cannot be seen in Fig. 8. We therefore present a logarithmic plot of the E615 data [15] on the normalized cross section in Fig. 9 which demonstrates that the Gaussian description is applicable for $q_T\lesssim$ (2–3) GeV but not beyond that. Since $4.05\le Q/\mathrm{GeV}\le 8.55$ and we need $q_T\ll Q$ for the TMD factorization to be applicable, one certainly cannot expect the approach to work beyond $q_T\lesssim$ (2–3) GeV. In Fig. 9 we limit ourselves to showing the data in the bin $0.2\le x_F\le 0.3$ only, because this x_F bin shows the limitations of the q_T description most clearly. The data sets from [15] in the other x_F bins shown in Fig. 8 happen to be less accurate at larger q_T and show deviations from the Gaussian ansatz less clearly. Depending on the energy, the Gaussian model was shown to work satisfactorily in DY up to $q_T\lesssim$ (2–3) GeV also in [117].

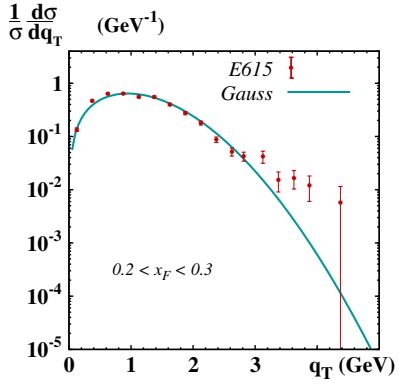

FIG. 9 (color online). The normalized cross section $(1/\sigma)(\mathrm{d}\sigma(q_T)/\mathrm{d}q_T)$ as a function of q_T for $0.2\le x_F\le 0.3$. The data are from Ref. [15]. The theoretical curves are from the LFCM with transverse momentum broadening effects estimated according to Eqs. (45) and (46). The logarithmic plot shows the limitation of the Gaussian description which works well for $q_T\lesssim$ (2–3) GeV.

At this point it is worth recalling that we neglect nuclear binding effects, which is justified for $q_T\lesssim 3$ GeV [14,16]. Thus, nuclear effects become important only beyond the range of q_T we are interested in. Moreover, since in the LFCM the $\langle k^2_{\perp,\mathrm{unp}}(x)\rangle$ are equal for u and d quarks in protons and neutrons, we do not need to distinguish protons and neutrons in the tungsten target.

To summarize, a parton-model description of cross section ratios in DY with the LFCM predictions for pion and nucleon unpolarized TMDs with the phenomenological estimate of transverse momentum broadening effects in Eqs. (45) and (46) works well for $s\sim$ (50–600) GeV^2 in the regions of $q_T\lesssim$ (2–3) GeV and $x_F\lesssim$ (0.7–0.8). Although the LFCM has its own limitations, this is the range of applicability of the TMD approach expected on general grounds, and we shall keep it in mind when embarking on the description of the Boer-Mulders effect in DY in the next section.

VIII. BOER-MULDERS EFFECT IN DY

In this section we describe the Boer-Mulders effect in the DY process. The treatment is in a large part parallel to the discussion of the unpolarized TMDs in Sec. VII.

A. Gaussian approximation and estimate of $k_\perp$ broadening for $h^{\perp a}_{1,h}(x,k^2_\perp)$

In analogy to the unpolarized TMDs in Eq. (50), also in the case of the Boer-Mulders functions it is convenient to recast the model predictions in terms of a Gaussian ansatz as follows:

$$h^{\perp a}_{1,h}(x,\boldsymbol{k}^2_\perp)=h^{\perp a}_{1,h}(x)\frac{\exp(-\boldsymbol{k}^2_\perp/\langle k^{2a/h}_{\perp,\mathrm{BM}}(x)\rangle)}{\pi\langle k^{2a/h}_{\perp,\mathrm{BM}}(x)\rangle},$$
$$\langle k^{2a/h}_{\perp,\mathrm{BM}}(x)\rangle=\frac{\int \mathrm{d}^2\boldsymbol{k}_\perp \boldsymbol{k}^2_\perp h^{\perp a}_{1,h}(x,\boldsymbol{k}^2_\perp)}{\int \mathrm{d}^2\boldsymbol{k}_\perp h^{\perp a}_{1,h}(x,\boldsymbol{k}^2_\perp)}. \quad (50)$$

The model results for $h^{\perp a}_{1,h}(x,\boldsymbol{k}^2_\perp)$ at the initial scale exhibit an approximate Gaussian $k_\perp$ behavior, see Fig. 4(b) in this work for the pion and [62] for the nucleon. This is well approximated by Eq. (47) thanks to the flexible

x-dependent Gaussian width. Moreover, also in the case of the Boer-Mulders functions the Gaussian ansatz will facilitate the estimate of transverse momentum broadening effects, as described below.

We remark that $h_{1,h}^{\perp a}(x) = \int \mathrm{d}^2\boldsymbol{k}_\perp h_{1,h}^{\perp a}(x,\boldsymbol{k}_\perp^2)$, though well defined in models, would have an involved QCD definition because one should "divide out" a power of transverse momentum from the correlator in Eq. (23). However, this quantity appears here merely as an "intermediate-step construct" and will be eliminated in favor of the (1) moment of the Boer-Mulders function in the final expression. We remark that treatments of the Boer-Mulders effect in DY in the Gaussian ansatz were reported e.g. in Refs. [79,81], though from our point of view the used Gaussian widths were sometimes chosen unacceptably small.

Using the Gaussian ansatz (50), one can analytically evaluate the convolution integral in the structure function (42). There are "infinitely many" possible ways to express the result. We choose to write it in terms of (1) moments of the Boer-Mulders function as follows:

$$F_{UU}^{\cos(2\phi)}(x_1,x_2,q_T) = \frac{1}{N_c}\sum_a e_a^2 h_{1,\pi}^{\perp(1)a}(x_1)_{\mathrm{DY}} h_{1,N}^{\perp(1)\bar{a}}(x_2)_{\mathrm{DY}} \frac{4M_\pi M_N}{\langle q_T^2\rangle_{\mathrm{BM}}} \frac{q_T^2 \exp(-q_T^2/\langle q_T^2\rangle_{\mathrm{BM}})}{\pi\langle q_T^2\rangle_{\mathrm{BM}}^2}, \tag{51}$$

$$F_{UU}^{\cos(2\phi)}(x_1,x_2) = \frac{1}{N_c}\sum_a e_a^2 h_{1,\pi}^{\perp(1)a}(x_1)_{\mathrm{DY}} h_{1,N}^{\perp(1)\bar{a}}(x_2)_{\mathrm{DY}} \frac{4M_\pi M_N}{\langle q_T^2\rangle_{\mathrm{BM}}}, \tag{52}$$

$$\langle q_T^2(x_1,x_2,s)\rangle_{\mathrm{BM}} = \langle k_{\perp,\mathrm{BM}}^{2a/\pi}(x_1)\rangle + \langle k_{\perp,\mathrm{BM}}^{2\bar{a}/N}(x_2)\rangle + \langle \delta k_{\perp,\,\mathrm{BM}}^2(s)\rangle. \tag{53}$$

One could also use $h_{1,h}^{\perp a}(x)$ or $h_{1,h}^{\perp(1/2)a}(x)$, or any other moment $h_{1,h}^{\perp(n)a}(x)$ defined analogously to Eq. (36), in order to express the structure functions in Eqs. (51) and (52). From the point of view of the Gaussian model, all such expressions would be equally acceptable. From phenomenological point of view, our choice in Eqs. (51) and (52) is preferred in the sense that this is the only case, where one deals with a single parameter $\langle \delta k_{\perp,\,\mathrm{BM}}^2(s)\rangle$ describing the accumulated $k_\perp$ broadening of the pion and nucleon Boer-Mulders functions. All other choices would require us to explicitly estimate the $k_\perp$ broadenings of the separate pion and nucleon Gaussian widths $\langle k_{\perp,\mathrm{BM}}^{2a/h}(x)\rangle$.

We find a good description of the data [14,15] on the q_T dependence of the Boer-Mulders effect in DY with

$$\langle \delta k_{\perp,\mathrm{BM}}^2(s)\rangle = 1.3\ \mathrm{GeV}^2 \quad \text{at } s \approx (470\text{–}540)\ \mathrm{GeV}^2 \tag{54}$$

in the range of q_T up to (2–3) GeV in which the Gaussian ansatz was shown to be applicable for unpolarized TMDs in Sec. VII B. DY data on the Boer-Mulders effect are available also for smaller center-of-mass energies s [11–15]. But we observe that we cannot describe these data using Eqs. (51) and (52). More precisely, descriptions of the data at smaller s are possible, but in a more limited range $q_T \lesssim 1$ GeV. We also found that different prescriptions to describe the structure function, say in terms of $h_{1,h}^{\perp a}(x)$ or $h_{1,h}^{\perp(1/2)a}(x)$, do not yield better descriptions.

These observations should not come as a surprise. None of such Gaussian ansatz descriptions can be expected to adequately describe the true QCD scale dependence of the Boer-Mulders functions. However, as we will show in the next section, the Gaussian ansatz is useful in a specific range of s and q_T with the understanding that $q_T \ll Q$. Only after the full CSS evolution for the Boer-Mulders functions become available will it be possible to undertake an attempt to describe Boer-Mulders data at all energies. Furthermore, it is important to compare the value of $\langle \delta k_{\perp,\,\mathrm{BM}}^2(s)\rangle$ in Eq. (51) with the broadening $\langle \delta k_{\perp,\mathrm{unp}}^2(s)\rangle = (1.6\text{–}1.8)\ \mathrm{GeV}^2$ of unpolarized TMDs in the same range of s. The accumulated $k_\perp$ broadening of the unpolarized TMDs is larger than that of the Boer-Mulders functions. This is a necessary (cf. footnote 1) and, in our case, numerically also sufficient condition to comply with positivity.

B. Comparison to the data

With the descriptions of the unpolarized structure function in Eqs. (45) and (49) and the Boer-Mulders structure function in Eqs. (51)–(54) we are now in the position to evaluate the coefficient ν in the angular distribution of the DY cross section in the Collins-Soper frame as defined through Eqs. (39) and (40).

We will compare to the data from the NA10 CERN experiment [14] and the E615 Fermi Lab experiment [15]. In both experiments secondary π^- beams were collided with nuclear targets. In the NA10 experiment [14] several beam energies were used. We will focus on the NA10 data taken with 286 GeV π^- beams impinging on tungsten or deuterium targets. The covered range of Q was $4.0 < Q < 8.5$ GeV and $Q > 11$ GeV to remove the influence of the J/ψ- and Υ-resonance regions. In order to discard the Berger-Brodsky higher twist effect [119] the cut $x_1 < 0.7$ was imposed. In the E615 Fermi Lab experiment [15] a 252 GeV π^- beam was collided with a tungsten target, and

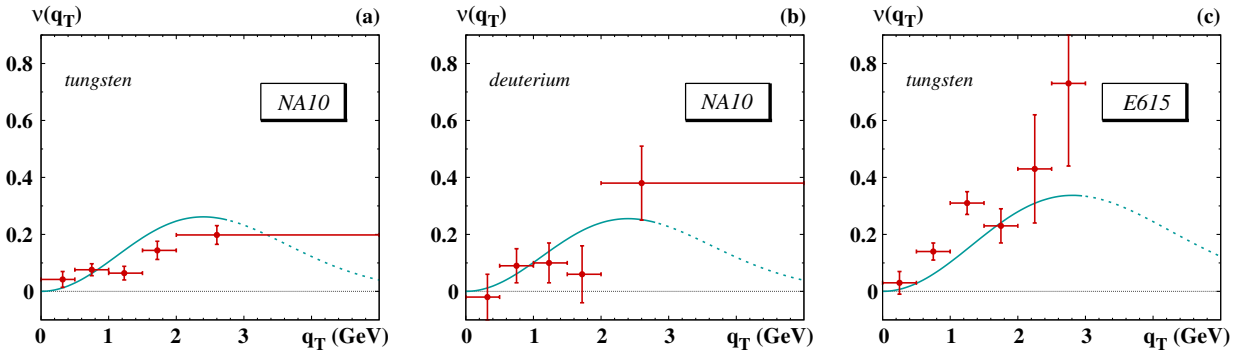

FIG. 10 (color online). The coefficient ν in the π^--nucleus DY angular distribution as a function of q_T. The data are from the NA10 CERN experiment with $E_{\rm beam} = 286$ GeV using tungsten (a) and deuterium (b) targets [14], and the E615 Fermi Lab experiment with $E_{\rm beam} = 252$ GeV using a tungsten target [15]. The theoretical curves are obtained using the LFCM predictions for the pion Boer-Mulders function obtained here, and the analog nucleon predictions from [64]. The solid (dotted) lines indicate where the TMD approach is applicable (not applicable).

the kinematic region $4.05 < Q < 8.55$ GeV between the J/ψ and Υ resonances was covered with $0.2 < x_1 < 1$. For our theoretical calculation we assume for simplicity $\langle Q^2 \rangle = 25$ GeV^2 as typical hard scale in both experiments.

Let us first discuss the q_T dependence of the coefficient ν. In the observable $\nu(q_T)$ the model input determines the overall normalization, while the q_T dependence is dictated by the Gaussian ansatz with the estimated $k_\perp$ broadening of the Boer-Mulder functions in Eqs. (51) and (54). In fact, more than testing the LFCM predictions, this comparison shows that the use of the Gaussian ansatz for the Boer-Mulders function with the estimated broadening (54) is compatible with the data, as can be seen in Fig. 10.

Several comments are in order. First, the NA10 tungsten data shown in Fig. 10(a) have a 10-times larger statistics than the NA10 deuterium data in Fig. 10(b). Within the statistical uncertainty of the data, no significant nuclear dependence was observed [14]. We exploited this observation when we defined our simplistic approach to estimate nuclear TMDs in Sec. VI A. Second, there seems to be a tendency in our approach to slightly overestimate the tungsten data from NA10 in Fig. 10(a), and to slightly underestimate the tungsten data from E615 in Fig. 10(c). The effect is not statistically significant. If it was, an explanation for that could be the fact that in the E615 data the Berger-Brodsky effect was included ($x_1 < 1$) but not in the NA10 data ($x_1 < 0.7$). Indications for the Berger-Brodsky effect were seen in the E615 experiment [15]. The slightly different energies in the two experiments could also play a role. Third, in Sec. VII B we learned that a Gaussian ansatz for unpolarized TMDs works well in the region $q_T \lesssim (2\text{–}3)$ GeV, but breaks down beyond that. Our descriptions of $\nu(q_T)$ in Fig. 10 are therefore certainly not valid for $q_T \gtrsim 3$ GeV and we have emphasized this region with dotted lines. Clearly, in the region $q_T \lesssim (2\text{–}3)$ GeV (indicated by solid lines) our description of $\nu(q_T)$ is compatible with the data. Fourth, it should be noted that the TMD approach in general requires $q_T \ll Q$. Thus, our results in Fig. 10 indicate that in the range $s \approx (470\text{–}540)$ GeV^2 $\nu(q_T)$ can be well described in the TMD approach with the Gaussian ansatz. Finally, we remark that our results safely comply with the model-independent positivity bound $|\frac{\nu}{2}| \leq 1$.

Next, we turn our attention to the x_1 dependence of the coefficient ν shown in Fig. 11. We recall that x_1 corresponds to the momentum fraction carried by the parton which originates from the pion. We use this variable here, because it is the only common kinematical variable (besides q_T) used to analyze data in both experiments [14,15]. The observable $\nu(x_1)$ provides a more stringent test of the model results, in the sense that the shapes of the theoretical curves in Fig. 11 are directly dictated by the LFCM predictions, although their overall normalizations are influenced through Eq. (52) by the choice of the parameter $\langle \delta k^2_{\perp,\,\rm BM}(s) \rangle$ in Eq. (54).

The comparison with the data in Fig. 11 is satisfactory. The most precise data set, namely the NA10 tungsten data in Fig. 11(a), may indicate that our model results somewhat overshoot the data in the region around $x_1 \sim 0.6$, but the effect is not significant. Even if it was, one should recall that the typical accuracy of the LFCM in applications to TMD phenomenology is (10–30)% [62,64]. The NA10 deuterium data [14] in Fig. 11(b) and the E615 tungsten data [14,15] in Fig. 11(c) have larger error bars, and our model results are compatible with them in the entire region of x_1.

It is important to keep in mind that the TMD approach is not applicable in the full range of x_1. In Sec. VII B we have seen that we can describe well the E615 data [15] on the (normalized) DY cross sections for $x_F \lesssim 0.7$, but not in the region $x_F \gtrsim 0.7$, where the Berger-Brodsky effect becomes increasingly significant. In the kinematics of the NA10 and E615 experiments this x_F region corresponds to $x_1 \gtrsim 0.76$, and we have indicated this region by dotted lines in Fig. 11. The Berger-Brodsky effect is not prominent in the NA10 data shown in Figs. 11(a) and 11(b). (Notice that the region

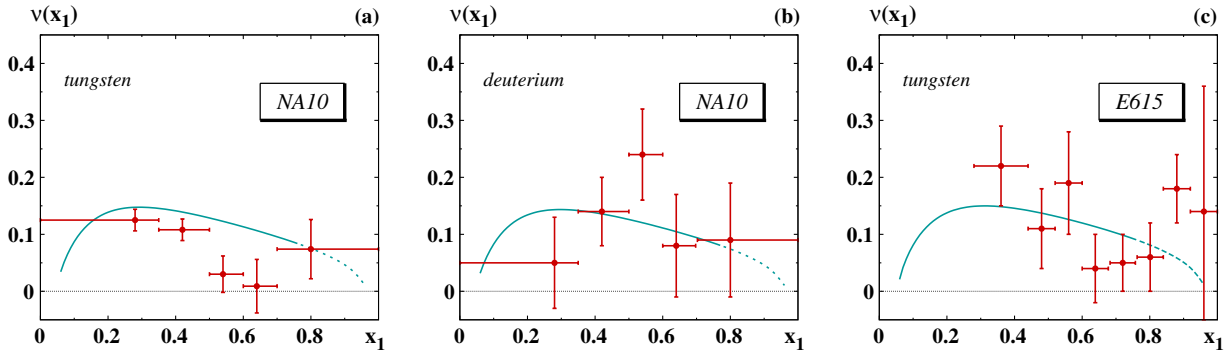

FIG. 11 (color online). The coefficient ν in the π^--nucleus DY angular distribution as function of x_1. The data are from the NA10 CERN experiment with $E_{\rm beam} = 286$ GeV using tungsten (a) and deuterium (b) targets [14], and the E615 Fermi Lab experiment with $E_{\rm beam} = 252$ GeV using a tungsten target [15]. The theoretical curves are obtained using the LFCM predictions for the pion Boer-Mulders function obtained here, and the corresponding nucleon predictions from [64]. The solid (dotted) lines indicate where the TMD approach is applicable (not applicable).

of $x_1 > 0.7$ was excluded in the NA10 analysis of ν as function of q_T which we discussed in Fig. 10.) However, there is an indication of this effect in the E615 data shown in Fig. 11(c).

To conclude, we observe that the predictions from the LFCM for the pion Boer-Mulders functions from this work and the nucleon from [64] are in good agreement with the NA10 and E615 data taken at $s \approx (470\text{–}540)$ GeV^2 [14,15]. The good agreement is based also on our use of the Gaussian ansatz in the TMD factorization approach, and the chosen method to estimate $k_\perp$-broadening effects, which corresponds to estimating CSS-evolution effects.

IX. SUMMARY AND OUTLOOK

In this work we studied the structure of the pion, as described in terms of the leading-twist TMDs $f_{1,\pi}(x, \boldsymbol{k}_\perp^2)$ and $h_{1,\pi}^\perp(x, \boldsymbol{k}_\perp^2)$, using a light-front constituent model where the pion is described in terms of the minimal Fock-state component consisting of a quark and antiquark. In a first step we determined the initial scale of this constituent approach to the pion, following a similar procedure commonly used in hadronic models with effective valence degrees of freedom. The resulting initial scale is about $\mu_0 \sim 0.5$ GeV and numerically similar to the initial scale in the case of the of constituent approach of the nucleon [62], supporting the validity of the constituent approach.

The $q\bar{q}$ LFWF of the pion was shown to involve two independent amplitudes describing the different orbital angular momentum components of the constituent quark and antiquark in the pion state [93,94]. In this work we derived a model-independent representation of leading-twist pion TMDs in terms of overlaps of light-front amplitudes which reveals the role of the different orbital angular-momentum components for the structure of the pion. We applied these expressions to a specific model, which has been successfully employed to describe the pion electromagnetic form factor [65,66]. Our predictions for the pion TMDs are in qualitative agreement with results from spectator and bag models [69–72] and lattice QCD [73]. We then evolved the model result for the collinear valence pion distribution function from the low hadronic scale to experimentally relevant scales, and demonstrated that it is in good agreement with available parametrizations. We observed that the $k_\perp$ dependence of the model TMDs is not exactly Gaussian, but can be usefully approximated by a Gaussian ansatz. In comparison with the model results for the nucleon Boer-Mulders function [63,64], we confirm that in LFCM approaches "all Boer-Mulders functions are alike," in the qualitative sense of Ref. [70].

As a phenomenological application, we studied the pion-nucleus induced Drell-Yan process. We reexpressed the model results in terms of an effective Gaussian ansatz for the $k_\perp$ dependence of TMDs, which is well supported (in the model and by the data), and incorporated phenomenologically the energy-dependent transverse momentum broadening effects. We have shown that the model predictions obtained in this way for the (normalized) cross sections, given in terms of the unpolarized pion and nucleon TMDs, compare very well with the data up to $q_T \lesssim (2\text{–}3)$ GeV for $x_F \lesssim 0.7$, which is basically the general range of applicability of the TMD factorization approach in DY.

We studied also the coefficient ν in the dilepton angular distribution in the Collins-Soper frame, which is described in the parton model [20,34] in terms of the pion and nucleon Boer-Mulders functions. We obtained a satisfactory description of available experimental data for $s \approx (470\text{–}540)$ GeV^2 and in the range of applicability of the TMD factorization approach established in our study of (normalized) cross sections.

The primary goal of this work was to extend the successful LFCM phenomenology of the nucleon to the pion case. The LFCM of the nucleon was shown to describe effects related to nucleon TMDs in SIDIS in the valence-x region within an accuracy of (10–30)% [62,64]. In this

work we demonstrated that the pion LFCM (in combination with the nucleon LFCM results) yields a similarly good description of pion-induced DY.

There are also several model-independent conclusions of our study. First, it is a remarkable fact that valence degrees of freedom are capable of successfully catching the main features of the pion-induced DY process, including (normalized) cross sections differential in $q_T \lesssim (2\text{–}3)$ GeV and $x_F \lesssim 0.7$ and the coefficient ν. This may indicate that the color entanglement effects discussed in [114] are not large, though more work is needed to shed further light in this respect. Second, the Gaussian ansatz is well capable of describing the Boer-Mulders effect in DY in the region $q_T \ll Q$, at least if one works in a limited range of energies. This point will be further clarified, when the CSS-evolution equations for the Boer-Mulders functions will be available and make possible a more comprehensive analysis of data at all energies.

Forthcoming or proposed pion-induced DY experiments will open new windows. The forthcoming COMPASS DY experiment [122,123], where a 190 GeV pion beam is available, is scheduled to start data taking this year and will include also polarized targets. The SPASCHARM experiment [124], where (10–70) GeV pion beams would be available, is in preparation at the IHEP facility in Protvino. The main focus of these experiments is to measure the single spin asymmetry in DY due to the other (besides Boer-Mulders function) T-odd TMD of the nucleon, namely the Sivers function [125], and test the predicted sign change between DIS and DY of this TMD [36] which was estimated to be feasible, see [126] for an early estimate. The sign change for the nucleon Boer-Mulders function can also be tested, but this requires measurements of several single spin asymmetries in DY, and it is less clear whether the measurements are feasible. In any case, these experiments will also give new insights into the structure of the pion. The present study in the LFCM will be extended to provide model predictions for these experiments.

ACKNOWLEDGMENTS

This work has been partially supported by the European Community Joint Research Activity "Study of Strongly Interacting Matter" (acronym HadronPhysics3, Grant No. 283286) under the Seventh Framework Programme of the European Community. The Feynman diagram in this paper was drawn using JaxoDraw [127]. This work was supported partially through GAUSTEQ (Germany and U.S. Nuclear Theory Exchange Program for QCD Studies of Hadrons and Nuclei) under Contract No. DE-SC0006758. The authors acknowledge the hospitality at the Physics Institute of the Gutenberg University Mainz where a part of this work was performed, and thank Marc Vanderhaeghen for fruitful discussions.

[1] J. C. Collins and D. E. Soper, Nucl. Phys. **B194**, 445 (1982).
[2] J. C. Collins, Acta Phys. Pol. B **34**, 3103 (2003).
[3] J. C. Collins, *Foundations of Perturbative QCD* (Cambridge University Press, Cambridge, England, 2011).
[4] R. D. Tangerman and P. J. Mulders, Phys. Rev. D **51**, 3357 (1995).
[5] A. Kotzinian, Nucl. Phys. **B441**, 234 (1995).
[6] P. J. Mulders and R. D. Tangerman, Nucl. Phys. **B461**, 197 (1996); **B484**, 538(E) (1997).
[7] D. Boer and P. J. Mulders, Phys. Rev. D **57**, 5780 (1998).
[8] A. Bacchetta, M. Diehl, K. Goeke, A. Metz, P. J. Mulders, and M. Schlegel, J. High Energy Phys. 02 (2007) 093.
[9] J. H. Christenson, G. S. Hicks, L. M. Lederman, P. J. Limon, B. G. Pope, and E. Zavattini, Phys. Rev. Lett. **25**, 1523 (1970).
[10] S. D. Drell and T. M. Yan, Phys. Rev. Lett. **25**, 316 (1970); **25**, 902(E) (1970); Ann. Phys. (N.Y.) **66**, 578 (1971).
[11] J. Badier *et al.* (NA3 Collaboration), Z. Phys. C **11**, 195 (1981).
[12] S. Palestini *et al.*, Phys. Rev. Lett. **55**, 2649 (1985).
[13] S. Falciano *et al.* (NA10 Collaboration), Z. Phys. C **31**, 513 (1986).
[14] M. Guanziroli *et al.* (NA10 Collaboration), Z. Phys. C **37**, 545 (1988).
[15] J. S. Conway *et al.*, Phys. Rev. D **39**, 92 (1989).
[16] P. Bordalo *et al.* (NA10 Collaboration), Phys. Lett. B **193**, 368 (1987); **193**, 373 (1987).
[17] W. J. Stirling and M. R. Whalley, J. Phys. G **19**, D1 (1993).
[18] P. L. McGaughey, J. M. Moss, and J. C. Peng, Annu. Rev. Nucl. Part. Sci. **49**, 217 (1999).
[19] P. E. Reimer, J. Phys. G **34**, S107 (2007).
[20] S. Arnold, A. Metz, and M. Schlegel, Phys. Rev. D **79**, 034005 (2009).
[21] W.-C. Chang and D. Dutta, Int. J. Mod. Phys. E **22**, 1330020 (2013).
[22] J.-C. Peng and J.-W. Qiu, Prog. Part. Nucl. Phys. **76**, 43 (2014).
[23] J. C. Collins and D. E. Soper, Nucl. Phys. **B193**, 381 (1981); **213**, 545(E) (1983).
[24] X. D. Ji, J. P. Ma, and F. Yuan, Phys. Rev. D **71**, 034005 (2005); Phys. Lett. B **597**, 299 (2004).
[25] J. C. Collins and A. Metz, Phys. Rev. Lett. **93**, 252001 (2004).
[26] M. G. Echevarria, A. Idilbi, and I. Scimemi, J. High Energy Phys. 07 (2012) 002.

[27] J. C. Collins, D. E. Soper, and G. Sterman, Nucl. Phys. **B250**, 199 (1985).
[28] S. M. Aybat and T. C. Rogers, Phys. Rev. D **83**, 114042 (2011).
[29] S. M. Aybat, J. C. Collins, J.-W. Qiu, and T. C. Rogers, Phys. Rev. D **85**, 034043 (2012).
[30] I. O. Cherednikov and N. G. Stefanis, Phys. Rev. D **77**, 094001 (2008); Nucl. Phys. **B802**, 146 (2008); Phys. Rev. D **80**, 054008 (2009); I. O. Cherednikov, A. I. Karanikas, and N. G. Stefanis, Nucl. Phys. **B840**, 379 (2010).
[31] A. Bacchetta and A. Prokudin, Nucl. Phys. **B875**, 536 (2013).
[32] M. G. Echevarría, A. Idilbi, A. Schäfer, and I. Scimemi, Eur. Phys. J. C **73**, 2636 (2013); M. G. Echevarría, A. Idilbi, and I. Scimemi, Phys. Lett. B **726**, 795 (2013); M. G. Echevarría, A. Idilbi, and I. Scimemi, Phys. Rev. D **90**, 014003 (2014); M. G. Echevarria, A. Idilbi, Z.-B. Kang, and I. Vitev, Phys. Rev. D **89**, 074013 (2014).
[33] A. A. Vladimirov, arXiv:1402.3182.
[34] D. Boer, Phys. Rev. D **60**, 014012 (1999).
[35] S. J. Brodsky, D. S. Hwang, and I. Schmidt, Phys. Lett. B **530**, 99 (2002).
[36] J. C. Collins, Phys. Lett. B **536**, 43 (2002).
[37] X. D. Ji and F. Yuan, Phys. Lett. B **543**, 66 (2002).
[38] S. J. Brodsky, D. S. Hwang, and I. Schmidt, Nucl. Phys. **B642**, 344 (2002).
[39] D. Boer, S. J. Brodsky, and D. S. Hwang, Phys. Rev. D **67**, 054003 (2003).
[40] A. V. Belitsky, X. Ji, and F. Yuan, Nucl. Phys. **B656**, 165 (2003).
[41] D. Boer, P. J. Mulders, and F. Pijlman, Nucl. Phys. **B667**, 201 (2003).
[42] C. S. Lam and W. K. Tung, Phys. Rev. D **18**, 2447 (1978); **21**, 2712 (1980).
[43] J. C. Collins, Phys. Rev. Lett. **42**, 291 (1979).
[44] E. Mirkes and J. Ohnemus, Phys. Rev. D **51**, 4891 (1995).
[45] A. Brandenburg, O. Nachtmann, and E. Mirkes, Z. Phys. C **60**, 697 (1993).
[46] A. Brandenburg, S. J. Brodsky, V. V. Khoze, and D. Mueller, Phys. Rev. Lett. **73**, 939 (1994).
[47] D. Boer, A. Brandenburg, O. Nachtmann, and A. Utermann, Eur. Phys. J. C **40**, 55 (2005).
[48] A. Brandenburg, A. Ringwald, and A. Utermann, Nucl. Phys. **B754**, 107 (2006).
[49] O. Nachtmann, arXiv:1401.7587.
[50] L. Y. Zhu *et al.* (NuSea Collaboration), Phys. Rev. Lett. **99**, 082301 (2007); **102**, 182001 (2009).
[51] S. Boffi, B. Pasquini, and M. Traini, Nucl. Phys. **B649**, 243 (2003).
[52] S. Boffi, B. Pasquini, and M. Traini, Nucl. Phys. **B680**, 147 (2004).
[53] B. Pasquini, M. Traini, and S. Boffi, Phys. Rev. D **71**, 034022 (2005).
[54] B. Pasquini, M. Pincetti, and S. Boffi, Phys. Rev. D **72**, 094029 (2005).
[55] B. Pasquini, M. Pincetti, and S. Boffi, Phys. Rev. D **76**, 034020 (2007).
[56] B. Pasquini and S. Boffi, Phys. Lett. B **653**, 23 (2007).
[57] B. Pasquini and S. Boffi, Phys. Rev. D **76**, 074011 (2007).
[58] S. Boffi and B. Pasquini, Riv. Nuovo Cimento **30**, 387 (2007).
[59] B. Pasquini, M. Pincetti, and S. Boffi, Phys. Rev. D **80**, 014017 (2009); S. Boffi and B. Pasquini, Mod. Phys. Lett. A **24**, 2882 (2009).
[60] C. Lorcé, B. Pasquini, and M. Vanderhaeghen, J. High Energy Phys. 05 (2011) 041.
[61] B. Pasquini, S. Cazzaniga, and S. Boffi, Phys. Rev. D **78**, 034025 (2008).
[62] S. Boffi, A. V. Efremov, B. Pasquini, and P. Schweitzer, Phys. Rev. D **79**, 094012 (2009); B. Pasquini, S. Boffi, and P. Schweitzer, Mod. Phys. Lett. A **24**, 2903 (2009).
[63] B. Pasquini and F. Yuan, Phys. Rev. D **81**, 114013 (2010).
[64] B. Pasquini and P. Schweitzer, Phys. Rev. D **83**, 114044 (2011).
[65] F. Schlumpf, Phys. Rev. D **50**, 6895 (1994).
[66] P. L. Chung, F. Coester, and W. N. Polyzou, Phys. Lett. B **205**, 545 (1988).
[67] T. Frederico, E. Pace, B. Pasquini, and G. Salmè, Phys. Rev. D **80**, 054021 (2009); Nucl. Phys. B, Proc. Suppl. **199**, 264 (2010).
[68] G. Salmé, E. Pace, and G. Romanelli, Few-Body Syst. **54**, 769 (2013); G. Salmé, E. Pace, and G. Romanelli, Few-Body Syst. **52**, 301 (2012).
[69] Z. Lu and B.-Q. Ma, Phys. Rev. D **70**, 094044 (2004).
[70] M. Burkardt and B. Hannafious, Phys. Lett. B **658**, 130 (2008).
[71] L. Gamberg and M. Schlegel, Phys. Lett. B **685**, 95 (2010).
[72] Z. Lu, B.-Q. Ma, and J. Zhu, Phys. Rev. D **86**, 094023 (2012).
[73] M. Engelhardt, B. Musch, P. Hägler, J. Negele, and A. Schäfer, arXiv:1310.8335; B. U. Musch, P. Hägler, M. Engelhardt, J. W. Negele, and A. Schäfer, Phys. Rev. D **85**, 094510 (2012).
[74] A. Bianconi and M. Radici, Phys. Rev. D **73**, 114002 (2006); **71**, 074014 (2005).
[75] Z. Lu and B.-Q. Ma, Phys. Lett. B **615**, 200 (2005).
[76] L. P. Gamberg and G. R. Goldstein, Phys. Lett. B **650**, 362 (2007).
[77] A. Sissakian, O. Shevchenko, A. Nagaytsev, O. Denisov, and O. Ivanov, Eur. Phys. J. C **46**, 147 (2006); A. Sissakian, O. Shevchenko, A. Nagaytsev, and O. Ivanov, Eur. Phys. J. C **59**, 659 (2009).
[78] V. Barone, Z. Lu, and B.-Q. Ma, Eur. Phys. J. C **49**, 967 (2007).
[79] B. Zhang, Z. Lu, B. Q. Ma, and I. Schmidt, Phys. Rev. D **77**, 054011 (2008).
[80] Z. Lu and I. Schmidt, Phys. Rev. D **81**, 034023 (2010).
[81] V. Barone, S. Melis, and A. Prokudin, Phys. Rev. D **82**, 114025 (2010).
[82] Z. Lu and I. Schmidt, Phys. Rev. D **84**, 094002 (2011).
[83] T. Liu and B.-Q. Ma, Eur. Phys. J. C **73**, 2291 (2013).
[84] T. Liu and B.-Q. Ma, Eur. Phys. J. C **72**, 2037 (2012).
[85] L. Chen, J.-h. Gao, and Z.-T. Liang, Phys. Rev. C **89**, 035204 (2014).
[86] C.-P. Chang and H.-N. Li, Phys. Lett. B **726**, 262 (2013).
[87] W. Broniowski, E. R. Arriola, and K. Golec-Biernat, Phys. Rev. D **77**, 034023 (2008).
[88] R. M. Davidson and E. Ruiz Arriola, Acta Phys. Pol. B **33**, 1791 (2002).

[89] A. Courtoy and S. Noguera, Phys. Lett. B **675**, 38 (2009).
[90] M. Gluck, E. Reya, and I. Schienbein, Eur. Phys. J. C **10**, 313 (1999).
[91] P. J. Sutton, A. D. Martin, R. G. Roberts, and W. J. Stirling, Phys. Rev. D **45**, 2349 (1992).
[92] A. D. Martin, W. J. Stirling, R. S. Thorne, and G. Watt, Eur. Phys. J. C **63**, 189 (2009).
[93] M. Burkardt, X. Ji, and F. Yuan, Phys. Lett. B **545**, 345 (2002).
[94] X.-D. Ji, J.-P. Ma, and F. Yuan, Eur. Phys. J. C **33**, 75 (2004).
[95] H. J. Melosh, Phys. Rev. D **9**, 1095 (1974).
[96] M. Glück, E. Reya, and A. Vogt, Z. Phys. C **53**, 651 (1992).
[97] J. F. Owens, Phys. Rev. D **30**, 943 (1984).
[98] M. B. Hecht, C. D. Roberts, and S. M. Schmidt, Phys. Rev. C **63**, 025213 (2001).
[99] M. Aicher, A. Schafer, and W. Vogelsang, Phys. Rev. Lett. **105**, 252003 (2010).
[100] K. Wijesooriya, P. E. Reimer, and R. J. Holt, Phys. Rev. C **72**, 065203 (2005).
[101] R. J. Holt and C. D. Roberts, Rev. Mod. Phys. **82**, 2991 (2010).
[102] M. Glück, E. Reya, and A. Vogt, Eur. Phys. J. C **5**, 461 (1998).
[103] M. Traini, A. Mair, A. Zambarda, and V. Vento, Nucl. Phys. **A614**, 472 (1997).
[104] A. Bacchetta, M. Boglione, A. Henneman, and P. J. Mulders, Phys. Rev. Lett. **85**, 712 (2000).
[105] A. Kotzinian, arXiv:0806.3804.
[106] D. Boer, Nucl. Phys. **B603**, 195 (2001).
[107] A. V. Kotikov and D. V. Peshekhonov, Phys. At. Nucl. **60**, 653 (1997); Eur. Phys. J. C **9**, 55 (1999).
[108] Y. Koike, J. Nagashima, and W. Vogelsang, Nucl. Phys. **B744**, 59 (2006).
[109] P. Ratcliffe, Nucl. Phys. **B223**, 45 (1983); V. Barone, A. Cafarella, C. Coriano, M. Guzzi, and P. Ratcliffe, Phys. Lett. B **639**, 483 (2006).
[110] W. Vogelsang and A. Weber, Phys. Rev. D **48**, 2073 (1993); A. P. Contogouris, B. Kamal, and Z. Merebashvili, Phys. Lett. B **337**, 169 (1994); B. Kamal, Phys. Rev. D **53**, 1142 (1996).
[111] D. Boer and W. Vogelsang, Phys. Rev. D **74**, 014004 (2006).
[112] H. Shimizu, G. F. Sterman, W. Vogelsang, and H. Yokoya, Phys. Rev. D **71**, 114007 (2005); A. Mukherjee and W. Vogelsang, Phys. Rev. D **73**, 074005 (2006).
[113] V. Ravindran and W. L. van Neerven, Nucl. Phys. **B589**, 507 (2000).
[114] M. G. A. Buffing and P. J. Mulders, Phys. Rev. Lett. **112**, 092002 (2014).
[115] B. Cox and P. K. Malhotra, Phys. Rev. D **29**, 63 (1984).
[116] U. D'Alesio and F. Murgia, Prog. Part. Nucl. Phys. **61**, 394 (2008).
[117] P. Schweitzer, T. Teckentrup, and A. Metz, Phys. Rev. D **81**, 094019 (2010).
[118] F. Landry, R. Brock, P. M. Nadolsky, and C. P. Yuan, Phys. Rev. D **67**, 073016 (2003).
[119] E. L. Berger and S. J. Brodsky, Phys. Rev. Lett. **42**, 940 (1979); E. L. Berger, Z. Phys. C **4**, 289 (1980).
[120] A. P. Bakulev, N. G. Stefanis, and O. V. Teryaev, Phys. Rev. D **76**, 074032 (2007).
[121] A. Bacchetta, D. Boer, M. Diehl, and P. J. Mulders, J. High Energy Phys. 08 (2008) 023.
[122] F. Gautheron *et al.* (COMPASS Collaboration), Report No. SPSC-P-340.
[123] C. Quintans (COMPASS Collaboration), J. Phys. Conf. Ser. **295**, 012163 (2011).
[124] V. V. Abramov, N. I. Belikov, Y. M. Goncharenko, V. N. Grishin, A. M. Davidenko, A. A. Derevshchikov, V. A. Kachanov, D. A. Konstantinov *et al.*, J. Phys. Conf. Ser. **295**, 012018 (2011).
[125] D. W. Sivers, Phys. Rev. D **41**, 83 (1990); Phys. Rev. D **43**, 261 (1991).
[126] A. V. Efremov, K. Goeke, S. Menzel, A. Metz, and P. Schweitzer, Phys. Lett. B **612**, 233 (2005).
[127] D. Binosi, J. Collins, C. Kaufhold, and L. Theussl, Comput. Phys. Commun. **180**, 1709 (2009).